Zhongxue Li · Haoyan Wei · Loc Vu-Quoc · Bassam A. Izzuddin · Xin Zhuo · Tianzong Li

A co-rotational triangular finite element for large deformation analysis of smooth, folded and multi-shells

Abstract   A six-node co-rotational curved triangular shell finite element with a novel rotation treatment for folded and multi-shell structures is presented. Different from other co-rotational triangular element formulations, rotations are not represented by axial (pseudo) vectors, but by components of polar (proper) vectors, of which additivity and commutativity lead to symmetry of the tangent stiffness matrices in both local and global coordinate systems. In the co-rotational local coordinate system, the two smallest components of the shell director are defined as the nodal rotational variables. Similarly, the two smallest components of each director in the global coordinate system are adopted as the global rotational variables for nodes located either on smooth shells or away from non-smooth shell intersections. At intersections of folded and multi-shells, global rotational variables are defined as three selected components of an orthogonal triad initially oriented along the global coordinate system axes. As such, the vectorial rotational variables enable simple additive update of all nodal variables in an incremental-iterative procedure, resulting in significant enhancement in computational efficiency for large deformation analysis. To alleviate membrane and shear locking phenomena, an assumed strain method is employed in obtaining the element tangent stiffness matrices and the internal force vector. The effectiveness of the presented co-rotational triangular shell element formulation is verified by analyzing several benchmark problems of smooth, folded, and multi-shell structures undergoing large displacements and large rotations.

Zhongxue Li (✉) · Xin Zhuo · Tianzong Li
Department of Civil Engineering, Zhejiang University, Hangzhou 310058, China
E-mail: lizx19993@zju.edu.cn; zhuoxin@zju.edu.cn; ltz@zju.edu.cn

Haoyan Wei
Livermore Software Technology, an ANSYS company, Livermore, CA 94551
E-mail: haoyan.wei@ansys.com

Loc Vu-Quoc
Aerospace Engineering, University of Illinois at Urbana-Champaign, Urbana, IL 61801, USA
E-mail: vql@illinois.edu

Bassam A. Izzuddin
Department of Civil and Environmental Engineering, Imperial College London, SW7 2BU, UK
E-mail:b.izzuddin@imperial.ac.uk

1 Introduction

Thin-walled shell structures have been widely used in engineering practice. Most of them consist of several regular shell elements interconnected along curvilinear junctions, such as pressure vessels, silos, liquid and gas storage tanks, tubular towers, branching and intersecting pipelines, etc. In most of such non-smooth shell structures, the adjacent elements are usually stiffly connected to each other [1-6]. Solving such shell structures with intersections, the so-called drilling rotation about the director field must be incorporated. Otherwise, the absence of a rotation component around the shell director will make it difficult to impose continuity at the branching points or provide a compatible connection with a beam model [7-9]. Several finite element formulations with drilling rotations have been developed [9-17]. However, incorporating the drilling rotation DOF at every node can lead to the singularity of the stiffness matrices in global coordinate system, as the stiffness due to drilling rotations is very low or nearly zero at nodes located away from the shell intersections. Therefore, special treatments must be adopted to cope with such numerical issues [18-19]. One way to avoid the difficulties associated with drilling DOFs is the adoption of solid-shell elements [20-24], where the nodal DOFs only consist of pure translational displacements, thus finite-rotation axial (pseudo) vectors and their complex update procedures are avoided by construction. However, solid-shell elements suffer from thickness locking which requires proper treatments, and in addition, each solid-shell element contains more DOFs than conventional shell elements, which results in higher computational cost.

To model folded and multi-shell structures, a six-node co-rotational curved triangular shell finite element formulation is presented in this paper. Instead of axial (pseudo) vectors used in conventional shell elements, the components of polar (proper) vectors are adopted to represent rotations, which are vectorial variables and lead to symmetric consistent tangent stiffness matrixes in both local and global coordinate systems. Similar to the vectorial rotational variables employed in the non-smooth co-rotational curved quadrilateral shell elements [25], the two smallest components of the shell director are defined as vectorial rotational variables for both smooth and

non-smooth shells in the local coordinate system. In the global coordinate system, the two smallest components of the shell director are defined as rotational variables at any node of smooth shells or any node away from intersections of non-smooth shells. Furthermore, at the intersection edges of non-smooth shells, instead of using axial rotation vectors, we define global rotational variables as three selected components of an orthogonal triad, including the two smallest components of one orientation vector and the smallest or second smallest component of another orientation vector. Such definition of rotational variables is different from the co-rotational curved triangular shell elements [26-27] previously developed for elastic and elasto-plastic smooth shell problems, where only the two smallest components of the shell director are defined as rotational variables in the global coordinate system. An assumed strain formulation based on the modified discrete strain gap method [28-29] is employed to alleviate locking in the co-rotational triangular shell element formulation. Through solving a number of challenging benchmark problems, the proposed six-node triangular shell element demonstrates satisfactory computational accuracy in modeling smooth, folded and multi-shell structures undergoing large displacements and large rotations[15,30-36]. Compared to other co-rotational shell element formulations[37-41], the present triangular shell element owns the following prominent features: (1) Instead of multiplicative update of rotational variables in conventional shell elements, all nodal variables of the proposed element are additive in a nonlinear incremental solution procedure, and hence the update of the element matrices are quite efficient; (2) Consistent tangent stiffness matrices are symmetric in both the local and global coordinate systems, which significantly improves computational efficiency and saves computer storage; (3) The element tangent stiffness matrix is updated using the total values of nodal variables in an incremental solution procedure, which potentially benefits dynamic analysis [32-43]. In addition, the present triangular co-rotational shell finite element is advantageous over the quadrilateral element shell element [25] when shell structures with complex geometries are encountered, which can be easily discretized using fast automatic triangular mesh generation techniques.

3

The outline of the paper is as follows. Section 2 presents the co-rotational framework and kinematics of the six-node curved triangular shell element, and describes the vectorial rotational variable-based finite rotation parameterization. Section 3 provides the local element response. Section 4 gives the transformation relationship between the local and global responses. To verify the reliability and computational accuracy of the proposed formulation, several benchmark examples are analyzed in Section 5, including one smooth semi-cylindrical shell, one perforated plate, and five folded-shell and multi-shell problems involving large displacements and large rotations. Concluding remarks are presented in Section 6.

2. Co-rotational framework and kinematics of the element

2.1 Description of the co-rotational framework

As depicted in Fig. 1, three coordinate systems are adopted for describing the kinematics of the curved triangular shell element:

1. The natural coordinate system, $(\xi, \ \eta, \ \varsigma)$ with the origin coincide with Node 1 of the six-node triangular shell element; ξ and η axes along two element edges intersect each other at the origin.

2. The global Cartesian system, $(X, \ Y, \ Z)$ with base vectors expressed as

    $\lfloor 1 \ \ 0 \ \ 0 \rfloor^{\mathrm{T}}, \lfloor 0 \ \ 1 \ \ 0 \rfloor^{\mathrm{T}}, \lfloor 0 \ \ 0 \ \ 1 \rfloor^{\mathrm{T}}.$

3. The co-rotational local Cartesian system, $(x, \ \ y, \ \ z)$ with the origin located at Node 1 of the six-node triangular shell element, and the base vectors $\mathbf{e}_x, \mathbf{e}_y, \mathbf{e}_z$ are to be described later in this section.
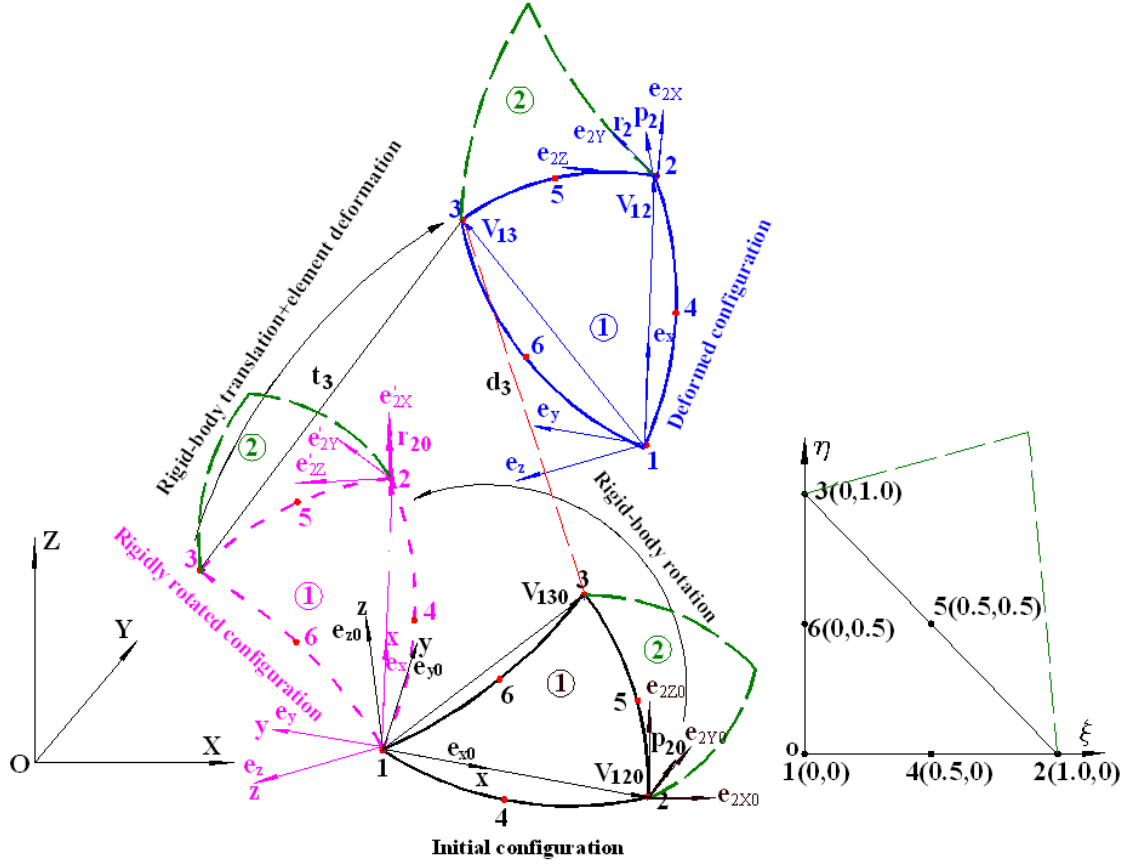
Fig. 1 The co-rotational framework and kinematics of the element

(Note: The vectors $\mathbf{t}_3$, $\mathbf{r}_{20}$ and $\mathbf{r}_2$ are associated with the local coordinate system o-x-y-z, whereas the vectors $\mathbf{d}_3$, $\mathbf{p}_{20}$, $\mathbf{p}_2$, $\mathbf{v}_{120}$, $\mathbf{v}_{12}$, $\mathbf{v}_{130}$, $\mathbf{v}_{13}$, $\mathbf{e}_{x0}$, $\mathbf{e}_{y0}$, $\mathbf{e}_{z0}$, $\mathbf{e}_x$, $\mathbf{e}_y$, $\mathbf{e}_z$, $\mathbf{e}_{2X0}$, $\mathbf{e}_{2Y0}$, $\mathbf{e}_{2Z0}$, $\mathbf{e}'_{2X}$, $\mathbf{e}'_{2Y}$, $\mathbf{e}'_{2Z}$, are associated with the global coordinate system O-X-Y-Z.)

In the initial configuration, the base vectors of the local coordinate system are defined as follows

$$\mathbf{e}_{x0} = \frac{\mathbf{v}_{120}}{\left|\mathbf{v}_{120}\right|}, \qquad \mathbf{e}_{y0} = \mathbf{e}_{z0} \times \mathbf{e}_{x0}, \qquad \mathbf{e}_{z0} = \frac{\mathbf{v}_{120} \times \mathbf{v}_{130}}{\left|\mathbf{v}_{120} \times \mathbf{v}_{130}\right|} \qquad (1\text{a,b,c})$$

where the subscript 0 denotes variables in the initial configuration, and the vector $\mathbf{v}_{1i0}(i = 2,3)$ pointing from Node 1 to Node i is expressed as

$$\mathbf{v}_{1i0} = \mathbf{X}_{i0} - \mathbf{X}_{10} \qquad (2)$$

5

in which $\mathbf{X}_{i0}$ is the initial position vector of Node i in the global coordinate system. Equation (1) indicates that, in the initial configuration, the direction of the local x-axis is coincident with the vector $\mathbf{V}_{120}$, whereas the z-axis is orthogonal to the plane defined by the vectors $\mathbf{V}_{120}$ and $\mathbf{V}_{130}$, and the y-axis is orthogonal to the x-z plane, which forms an orthogonal triad of unit vectors.

Similarly, the updated base vectors of the local coordinate system in the current configuration is defined as

$$\mathbf{e}_x = \frac{\mathbf{v}_{12}}{|\mathbf{v}_{12}|}, \qquad \mathbf{e}_y = \mathbf{e}_z \times \mathbf{e}_x, \qquad \mathbf{e}_z = \frac{\mathbf{v}_{12} \times \mathbf{v}_{13}}{|\mathbf{v}_{12} \times \mathbf{v}_{13}|} \qquad \text{(3a,b,c)}$$

where the vectors $\mathbf{v}_{1i}$ is defined as follows

$$\mathbf{v}_{1i} = \mathbf{v}_{1i0} + \mathbf{d}_i - \mathbf{d}_1 \qquad (4)$$

in which $\mathbf{d}_i$ denotes the displacement of Node i, and $\mathbf{v}_{1i0}$ is defined in (2).

Since the Mindlin-Reissner kinematics is adopted, both translational and rotational DOFs (Degrees of freedom) in the global coordinate system need to be considered at every node i. Accordingly, we define the vector $\mathbf{u}_g^{\mathrm{T}}$ that consists of all global DOFs for each element:

$$\mathbf{u}_g^{\mathrm{T}} = \left\lfloor \mathbf{d}_1^{\mathrm{T}} \quad \mathbf{n}_{g1}^{\mathrm{T}} \quad \dots \quad \mathbf{d}_i^{\mathrm{T}} \quad \mathbf{n}_{gi}^{\mathrm{T}} \quad \dots \quad \mathbf{d}_6^{\mathrm{T}} \quad \mathbf{n}_{g6}^{\mathrm{T}} \right\rfloor \qquad (5)$$

where

$$\mathbf{d}_i^{\mathrm{T}} = \left\lfloor U_i \quad V_i \quad W_i \right\rfloor \qquad (6)$$

which contains the three global translational DOFs associated with node i, and $\mathbf{n}_{gi}^{\mathrm{T}}$ in Equation (5) is a vector of global rotational DOFs associated with node i, which contains two or three components depending on the location of node i. Specifically, we consider the following two scenarios:

Case (I): If the considered node i is located at the intersection of non-smooth shells, such as folded and multi-shell structures, then three global rotational DOFs are chosen:

$$\mathbf{n}_{gi}^{\mathrm{T}} = \lfloor e_{iy,n} \quad e_{iy,m} \quad e_{iz,n} \rfloor \tag{7}$$

where $\left| e_{iy,l} \right| \geq \left| e_{iy,m} \right|$, $\left| e_{iy,l} \right| \geq \left| e_{iy,n} \right|$, and $\left| e_{iz,m} \right| \geq \left| e_{iz,n} \right|$. Evidently, $e_{iy,m}$ and $e_{iy,n}$ are the two

smallest components of vector $\mathbf{e}_{iy}$ at Node i, whereas $e_{iz,n}$ is either the smallest or next to the

smallest component of vector $\mathbf{e}_{iz}$ at Node i. These vectorial rotational variables are chosen such

that the signs of $e_{iy,l}$ and $e_{iz,m}$ are kept unchanged during the current incremental loading step. It

is also noted that n, m, and l in $\{n,m,l\}$ (the circular permutation of $\{X,Y,Z\}$) can take different

values at different nodes, and these values can change at different loading steps in an incremental

solution procedure. At the current loading step, if $e_{iy,n}, e_{iy,m}$, and $e_{iz,n}$ are known, then the

other three components of $\mathbf{e}_{iy}$ and $\mathbf{e}_{iz}$ can be readily obtained as follows:

$$\| \mathbf{e}_{iy} \|^2 = e_{iy,l}^2 + e_{iy,m}^2 + e_{iy,n}^2 = 1 \Rightarrow e_{iy,l} = s_1 \sqrt{1 - (e_{iy,m}^2 + e_{iy,n}^2)} \tag{8a}$$

$$\| \mathbf{e}_{iz} \|^2 = e_{iz,l}^2 + e_{iz,m}^2 + e_{iz,n}^2 = 1 \Rightarrow e_{iz,m} = s_3 \sqrt{1 - (e_{iz,n}^2 + e_{iz,l}^2)} \tag{8b}$$

$$\left. \begin{array}{l} \left\| \mathbf{e}_{iy} \right\|^2 = 1 \\ \left\| \mathbf{e}_{iz} \right\|^2 = 1 \\ \mathbf{e}_{iy}^{\mathrm{T}} \mathbf{e}_{iz} = 0 \end{array} \right\} \Rightarrow e_{iz,l} = \frac{-e_{iy,l} e_{iy,n} e_{iz,n} + s_2 e_{iy,m} \sqrt{1 - e_{iy,n}^2 - e_{iz,n}^2}}{1 - e_{iy,n}^2} \tag{8c}$$

where the sign symbol $s_2 = -s_1 \cdot s_3$, and (s_1, s_3) have the same signs as those of $e_{iy,l}$ and

$e_{iz,m}$ in the previous loading step, respectively, which is equal to either 1 or –1. Finally, the vector

$\mathbf{e}_{ix}$ is simply the cross-product of $\mathbf{e}_{iy}$ and $\mathbf{e}_{iz}$:

$$\mathbf{e}_{ix} = \mathbf{e}_{iy} \times \mathbf{e}_{iz} \tag{9}$$

For convenience, we choose to initialize $\mathbf{e}_{ix}$, $\mathbf{e}_{iy}$, $\mathbf{e}_{iz}$ in the undeformed configuration to be

coincident to the base vectors of the global Cartesian system as follows:

$$\mathbf{e}_{ix0}^{\mathrm{T}} = \lfloor 1 \quad 0 \quad 0 \rfloor, \quad \mathbf{e}_{iy0}^{\mathrm{T}} = \lfloor 0 \quad 1 \quad 0 \rfloor, \quad \mathbf{e}_{iz0}^{\mathrm{T}} = \lfloor 0 \quad 0 \quad 1 \rfloor \quad (10\text{a,b,c})$$

It is noteworthy to mention that, the orthogonal triad of unit vectors initialized in the above equations (10a,b,c) can have different orientations at each node during the incremental loading procedure as indicated in Equations (8-9), whereas the co-rotational local coordinate system's base vectors, which are initialized and updated according to Equation (1) and Equation (3), are uniquely defined within each element domain and should be considered as an element-wise orthogonal triad.

Case (II): If a smooth shell is modelled, or if the considered node i is away from intersections of non-smooth shells, then there are two global rotational DOFs in $\mathbf{n}_{gi}$:

$$\mathbf{n}_{gi}^{\mathrm{T}} = \lfloor p_{i,n} \quad p_{i,m} \rfloor \quad (11)$$

where ($p_{i,n}$, $p_{i,m}$) denote the two smallest global components of the shell director at node i, and the remaining third component of the director is defined as

$$p_{i,l} = s_4 \sqrt{1 - p_{i,n}^2 - p_{i,m}^2} \qquad i = 1,2,...,6 \quad (12)$$

where $s_4 = \pm 1$ takes the same sign as used for $p_{i,l}$ in the previous loading step, and $\{n,m,l\}$ denotes the circular permutation of $\{X,Y,Z\}$.

For each six-node shell element, thirty nodal DOFs are considered in the co-rotational local coordinate system:

$$\mathbf{u}_L^{\mathrm{T}} = \lfloor \mathbf{t}_1^{\mathrm{T}} \quad \mathbf{\theta}_1^{\mathrm{T}} \quad ... \quad \mathbf{t}_i^{\mathrm{T}} \quad \mathbf{\theta}_i^{\mathrm{T}} \quad ... \quad \mathbf{t}_6^{\mathrm{T}} \quad \mathbf{\theta}_6^{\mathrm{T}} \rfloor \quad (13)$$

which includes the local translational displacement vector of Node i

$$\mathbf{t}_i^{\mathrm{T}} = \lfloor u_i \quad \upsilon_i \quad w_i \rfloor \quad (14)$$

and the corresponding local rotational variables:

$$\mathbf{\theta}_i^{\mathrm{T}} = \lfloor r_{ix} \quad r_{iy} \rfloor \quad (15)$$

where r_{ix} and r_{iy} are two components of the nodal shell director along the local x- and y -axes, respectively.

An explicit relationship between the local translational displacement $\mathbf{t}_i$ in (14) and the global translational displacement $\mathbf{d}_i$ in (6) is given as:

$$\mathbf{t}_i = \mathbf{R}\mathbf{d}_i + (\mathbf{R} - \mathbf{R}_0)\mathbf{v}_{1i0} \tag{16}$$

where $\mathbf{v}_{1i0} = \mathbf{X}_{i0} - \mathbf{X}_{10}$ ($i = 1, 2, ..., 6$), $\mathbf{R}_0$ and $\mathbf{R}$ are rotation matrices defined in the initial and current configurations, respectively:

$$\mathbf{R}_0{}^{\mathrm{T}} = \begin{bmatrix} \mathbf{e}_{x0} & \mathbf{e}_{y0} & \mathbf{e}_{z0} \end{bmatrix}, \qquad \mathbf{R}^{\mathrm{T}} = \begin{bmatrix} \mathbf{e}_x & \mathbf{e}_y & \mathbf{e}_z \end{bmatrix} \tag{17a,b}$$

in which the base vectors have been defined previously in Equations (1) and (3). In transforming the nodal displacements from the global to local coordinate systems according to Eq.(16), the initial local reference system is first rotated to the same orientation of the current local reference system, and then the local translations excluding rigid body rotations are measured with reference to this rotated configuration, as illustrated in Fig. 1.

If node i is away from non-smooth shell intersections, the relationship between the local and global components of the shell director is expressed as:

$$\mathbf{r}_{i0} = \mathbf{R}_0\mathbf{p}_{i0}, \qquad \mathbf{r}_i = \mathbf{R}\mathbf{p}_i \tag{18a,b}$$

where the subscript 0 denotes variables in the initial configuration as mentioned in Equation (1), i.e., $\mathbf{p}_{i0}$ and $\mathbf{p}_i$ contain the initial and current global components of the shell director at Node i, respectively; $\mathbf{r}_{i0}$ and $\mathbf{r}_i$ contain the initial and current local components of the shell director at Node i, respectively.

On the other hand, at intersections of non-smooth shells, the relationship between the local and global components of the shell director at node i is as follows

$$\mathbf{r}_{i0} = \mathbf{R}_0 \mathbf{p}_{i0}, \qquad \mathbf{r}_i = \mathbf{R}\mathbf{R}_i^{\mathrm{T}}\mathbf{R}_{i0}\mathbf{p}_{i0} \qquad\qquad (19\text{a,b})$$

where the rotation matrices $\mathbf{R}_{i0}$ and $\mathbf{R}_i$ in the initial and current configurations are defined as

$$\mathbf{R}_{i0}^{\mathrm{T}} = \begin{bmatrix} \mathbf{e}_{ix0} & \mathbf{e}_{iy0} & \mathbf{e}_{iz0} \end{bmatrix}, \quad \mathbf{R}_i^{\mathrm{T}} = \begin{bmatrix} \mathbf{e}_{ix} & \mathbf{e}_{iy} & \mathbf{e}_{iz} \end{bmatrix} \qquad (20\text{a,b})$$

where the orthogonal triad of unit vectors $\mathbf{e}_{ix0}$, $\mathbf{e}_{iy0}$, $\mathbf{e}_{iz0}$ follows the definition in Equation (10a,b,c), and $\mathbf{e}_{ix}$, $\mathbf{e}_{iy}$, $\mathbf{e}_{iz}$ follow the Equations (8-9).

2.2 Kinematics of the curved triangular shell element

To describe the geometry and deformation of the six-node triangular shell element, the following quadratic Lagrangian interpolation functions are adopted:

$$N_1 = (1-\xi-\eta)(1-2\xi-2\eta), \quad N_2 = \xi(2\xi-1), \quad N_3 = \eta(2\eta-1) \qquad (21\text{a,b,c})$$

$$N_4 = 4\xi(1-\xi-\eta), \quad N_5 = 4\xi\eta, \quad N_6 = 4\eta(1-\xi-\eta) \qquad (21\text{d,e,f})$$

where (ξ,η) are the natural coordinates, as depicted in Fig.1. Based on the iso-parametric approximation approach, the same set of shape functions defined in (21) are adopted to approximate the local coordinates $\mathbf{x}^{\mathrm{T}} = \lfloor x \quad y \quad z \rfloor$ and global coordinates $\mathbf{X}^{\mathrm{T}} = \lfloor X \quad Y \quad Z \rfloor$ of any point on the shell element mid-surface, as follows

$$\mathbf{x} = \sum_{i=1}^{6} N_i(\xi,\eta)\mathbf{x}_i, \qquad \mathbf{X} = \sum_{i=1}^{6} N_i(\xi,\eta)\mathbf{X}_i \qquad (22\text{a,b})$$

In addition, the local displacement fields $\mathbf{t}^{\mathrm{T}} = \lfloor u \quad v \quad w \rfloor$, and the local rotation fields $\bar{\mathbf{r}}_{\mathrm{h}}^{\mathrm{T}} = \lfloor r_x \quad r_y \rfloor$ as approximated as follows

$$\mathbf{t} = \sum_{i=1}^{6} N_i(\xi, \eta) \mathbf{t}_i \tag{23}$$

$$\bar{\mathbf{r}}_{\mathrm{h}} = \sum_{i=1}^{6} N_i(\xi, \eta) \boldsymbol{\theta}_i \tag{24}$$

where $\mathbf{t}_i$ and $\boldsymbol{\theta}_i$ are the nodal translational and rotational variables defined in (14) and (15), respectively; $\mathbf{x}_i$ and $\mathbf{X}_i$ are the local and global nodal coordinate of node i on the shell mid-surface.

The global components of the initial shell director at node i is obtained as the cross-product of the tangent lines along two natural coordinate axes:

$$\bar{\mathbf{p}}_{i0}^e = \frac{\partial \mathbf{X}_0}{\partial \xi} \times \frac{\partial \mathbf{X}_0}{\partial \eta} \bigg|_{(\xi_i, \eta_i)} \tag{25}$$

where (ξ_i, η_i) takes the natural coordinates of Node i (referred to Fig. 1), the subscript 0 refers to variables in the initial configuration as mentioned previously, and the superscript e denotes the element index, i.e., $e = 1, 2, ..., NE$, NE is the total number of shell elements in the discretized model.

Spurious slope discontinuities can appear at nodal positions between adjacent elements in smooth shells, which is due to the piecewise polynomial interpolation within each element domain. To address this issue, the mean value of the shell directors from surrounding elements of node i is adopted:

$$\mathbf{p}_{i0} = \frac{\sum_{e \in S_i} \bar{\mathbf{p}}_{i0}^e / \left| \bar{\mathbf{p}}_{i0}^e \right|}{\left\| \sum_{e \in S_i} \bar{\mathbf{p}}_{i0}^e / \left| \bar{\mathbf{p}}_{i0}^e \right| \right\|} \tag{26}$$

where the element set S_i contains all shell elements connected with Node i.

To model non-smooth shell intersections in folded and multi-shell structures, however, the directors of multiple elements evaluated at the shared node i should be considered independent to each other. Hence, three global nodal rotational DOFs are then required at the intersections where physical slope discontinuities exist. Furthermore, the director at node i in the current configuration is updated as:

$$\mathbf{p}_i = \mathbf{R}_i^{\mathrm{T}} \mathbf{R}_{i0} \mathbf{p}_{i0} \tag{27}$$

where the rotation matrices $\mathbf{R}_{i0}$ and $\mathbf{R}_i$ are defined in Equation (20), which consist of orthogonal triad of unit vectors in the initial and current configurations, respectively.

3 Local element formulation

The total potential energy functional of a curved shell element is defined as

$$\Pi = \frac{1}{2} \int_{\mathrm{V}} \boldsymbol{\varepsilon}^{\mathrm{T}} \mathbf{D}_1 \boldsymbol{\varepsilon} \, \mathrm{dV} + \frac{1}{2} \int_{\mathrm{V}} \boldsymbol{\gamma}^T \mathbf{D}_2 \boldsymbol{\gamma} \, \mathrm{dV} - \mathrm{W}_e \tag{28}$$

where $\boldsymbol{\varepsilon}$ is the in-plane strain, $\boldsymbol{\gamma}$ is the transverse shear strain, V is the element volume, W_e is the work done by external forces, $\mathbf{D}_1$ and $\mathbf{D}_2$ are the elastic-moduli matrices:

$$\mathbf{D}_1 = \frac{\mathrm{E}}{1-\mu^2} \begin{bmatrix} 1 & \mu & 0 \\ \mu & 1 & 0 \\ 0 & 0 & \dfrac{1+\mu}{2} \end{bmatrix}, \quad \mathbf{D}_2 = k_1 \frac{\mathrm{E}}{2(1+\mu)} \begin{bmatrix} 1 & 0 \\ 0 & 1 \end{bmatrix} \tag{29a,b}$$

where k_1 is the shear factor, $k_1 = \dfrac{5}{6}$ or $k_1 = \dfrac{\pi^2}{12}$, E is Young's modulus, and μ is the Poisson's ratio.

For convenience, the in-plane strain vector $\boldsymbol{\varepsilon}$ is split into two parts, including a membrane strain vector $\boldsymbol{\varepsilon}_m$ and a bending strain vector $z_l \boldsymbol{\chi}$, where z_l is defined as

$$z_l = \frac{1}{2} \zeta a \tag{30}$$

in which a denotes the shell thickness.

As a result of the strain splitting operation, Equation (28) can be rewritten as

$$\Pi = \frac{1}{2} \int_V (\boldsymbol{\varepsilon}_m + z_l \boldsymbol{\chi})^T \mathbf{D}_1 (\boldsymbol{\varepsilon}_m + z_l \boldsymbol{\chi}) dV + \frac{1}{2} \int_V \boldsymbol{\gamma}^T \mathbf{D}_2 \boldsymbol{\gamma} \, dV - W_e \tag{31}$$

where

$$\boldsymbol{\varepsilon}_m^T = \left\lfloor \varepsilon_{xx} \quad \varepsilon_{yy} \quad \gamma_{xy} \right\rfloor = \left\lfloor \frac{\partial u}{\partial x} \quad \frac{\partial \upsilon}{\partial y} \quad \frac{\partial u}{\partial y} + \frac{\partial \upsilon}{\partial x} \right\rfloor \tag{32a}$$

$$\boldsymbol{\chi}^T = \left\lfloor \frac{\partial (r_x - r_{x0})}{\partial x} \quad \frac{\partial (r_y - r_{y0})}{\partial y} \quad \frac{\partial (r_x - r_{x0})}{\partial y} + \frac{\partial (r_y - r_{y0})}{\partial x} \right\rfloor \tag{32b}$$

$$\boldsymbol{\gamma}^T = \left\lfloor \gamma_{xz} \quad \gamma_{yz} \right\rfloor = \left\lfloor \frac{\partial w}{\partial x} + r_x - r_{x0} \quad \frac{\partial w}{\partial y} + r_y - r_{y0} \right\rfloor \tag{32c}$$

In the above equations, all the spatial derivatives with respect to the local coordinates can be calculated from

$$\left\{ \begin{array}{c} \dfrac{\partial}{\partial x} \\ \dfrac{\partial}{\partial y} \\ \dfrac{\partial}{\partial z} \end{array} \right\} = \mathbf{J}^{-1} \left\{ \begin{array}{c} \dfrac{\partial}{\partial \xi} \\ \dfrac{\partial}{\partial \eta} \\ \dfrac{\partial}{\partial \zeta} \end{array} \right\}, \qquad \mathbf{J} = \left[\begin{array}{ccc} \dfrac{\partial x}{\partial \xi} & \dfrac{\partial y}{\partial \xi} & \dfrac{\partial z}{\partial \xi} \\ \dfrac{\partial x}{\partial \eta} & \dfrac{\partial y}{\partial \eta} & \dfrac{\partial z}{\partial \eta} \\ \dfrac{\partial x}{\partial \zeta} & \dfrac{\partial y}{\partial \zeta} & \dfrac{\partial z}{\partial \zeta} \end{array} \right] \tag{33a,b}$$

Taking the variation of the potential energy functional Π with respect to the local nodal variables $\mathbf{u}_L$ and enforcing it to be zero yields the following equation:

$$\delta\Pi = [\int_V (\boldsymbol{\varepsilon}_m + z_l \boldsymbol{\chi})^T \mathbf{D}_1 (\mathbf{B}_m + z_l \mathbf{B}_b) dV + \int_V \boldsymbol{\gamma}^T \mathbf{D}_2 \mathbf{B}_\gamma \, dV] \delta\mathbf{u}_L - \mathbf{f}_{ext} \delta\bar{\mathbf{u}} = 0 \tag{34}$$

where the gradient matrices $\mathbf{B}_m$, $z_l \mathbf{B}_b$, and $\mathbf{B}_\gamma$ are associated with the first-order derivatives of

the membrane strain $\boldsymbol{\varepsilon}_m$, bending strain $z_l\boldsymbol{\chi}$, and the out-of-plane shear strain $\boldsymbol{\gamma}$, respectively. Detailed expressions of these matrices are given in Appendix A.

The internal force vector in the local coordinate system is given by

$$\mathbf{f} = \mathbf{f}_{ext} = \int_V (\mathbf{B}_m + z_l\mathbf{B}_b)^T \mathbf{D}_1(\boldsymbol{\varepsilon}_m + z_l\boldsymbol{\chi})dV + \int_V \mathbf{B}_\gamma^T \mathbf{D}_2\,\boldsymbol{\gamma}dV$$

$$= \int_V (\mathbf{B}_m^T\mathbf{D}_1\boldsymbol{\varepsilon}_m + z_l^2\mathbf{B}_b^T\mathbf{D}_1\boldsymbol{\chi})dV + \int_V \mathbf{B}_\gamma^T\mathbf{D}_2\boldsymbol{\gamma}\,dV \tag{35}$$

By differentiating the internal force vector $\mathbf{f}$ with respect to the local nodal variables $\mathbf{u}_L$, the consistent tangent stiffness matrix of the 6-node curved triangular shell element is obtained

$$\mathbf{k}_T = \int_V [\mathbf{B}_m^T\mathbf{D}_1\mathbf{B}_m + z_l^2\mathbf{B}_b^T\mathbf{D}_1\mathbf{B}_b + \mathbf{B}_\gamma^T\mathbf{D}_2\mathbf{B}_\gamma]dV \tag{36}$$

Equations (35) and (36) represent the conforming formulation for the six-node curved triangular shell element in the local coordinate system. Due to the commutativity of the local nodal variables in calculating the second-order derivatives of the energy functional Π, the resulting consistent element tangent stiffness matrix $\mathbf{k}_T$ is symmetric.

The conforming element formulations in equations(35) and (36) suffer from membrane and shear locking and thus cannot provide satisfactory performance in solving thin shell problems. enlightened by the discrete strain gap method proposed by Koschnick et al.[28] and Bletzinger et al.[29], a new assumed strain method is proposed to alleviate the membrane and shear locking in calculating the internal force and element tangent stiffness matrix herein:

$$\mathbf{f} = \int_V \left(\tilde{\mathbf{B}}_m^T\mathbf{D}_1\tilde{\boldsymbol{\varepsilon}}_m + z_l^2\mathbf{B}_b^T\mathbf{D}_1\boldsymbol{\chi}\right)dV + \int_V \tilde{\mathbf{B}}_\gamma^T\mathbf{D}_2\tilde{\boldsymbol{\gamma}}\,dV \tag{37}$$

$$\mathbf{k}_T = \int_V \left(\tilde{\mathbf{B}}_m^T\mathbf{D}_1\tilde{\mathbf{B}}_m + z_l^2\mathbf{B}_b^T\mathbf{D}_1\mathbf{B}_b + \tilde{\mathbf{B}}_\gamma^T\mathbf{D}_2\tilde{\mathbf{B}}_\gamma\right)dV \tag{38}$$

where $\tilde{\mathbf{B}}_m$ and $\tilde{\mathbf{B}}_\gamma$ are respectively the first-order derivatives of the assumed membrane strains $\tilde{\boldsymbol{\varepsilon}}_m$ and the assumed transverse shear strain vector $\tilde{\boldsymbol{\gamma}}$ with respect to the local nodal variable vector

$\mathbf{u}_L$,the detailed expressions of them are given in Appendix A. It is noteworthy to mention that, after introducing the assumed strains, the consistent local element tangent stiffness matrix in (38) remains symmetric.

The discrete membrane gaps are evaluated by integrating the membrane strains over the element domain,

$$\Delta \bar{u}_{mxi} = \int_{\xi_1}^{\xi_i} \varepsilon_{xx} J_{1,1} d\xi \Big|_{\eta=\eta_i} + \int_{\eta_1}^{\eta_i} \varepsilon_{xx} J_{2,1} d\eta \Big|_{\xi=\xi_i} \qquad (39a)$$

$$\Delta \bar{\upsilon}_{myi} = \int_{\xi_1}^{\xi_i} \varepsilon_{yy} J_{1,2} d\xi \Big|_{\eta=\eta_i} + \int_{\eta_1}^{\eta_i} \varepsilon_{yy} J_{2,2} d\eta \Big|_{\xi=\xi_i} \qquad (39b)$$

$$\Delta \bar{u}_{mxyi} = \int_{\xi_1}^{\xi_i} \frac{\partial u}{\partial y} J_{1,2} d\xi \Big|_{\eta=\eta_i} + \int_{\eta_1}^{\eta_i} \frac{\partial u}{\partial y} J_{2,2} d\eta \Big|_{\xi=\xi_i} \qquad (39c)$$

$$\Delta \bar{\upsilon}_{mxyi} = \int_{\xi_1}^{\xi_i} \frac{\partial \upsilon}{\partial x} J_{1,1} d\xi \Big|_{\eta=\eta_i} + \int_{\eta_1}^{\eta_i} \frac{\partial \upsilon}{\partial x} J_{2,1} d\eta \Big|_{\xi=\xi_i} \qquad (39d)$$

and the assumed membrane strains are calculated as

$$\bar{\varepsilon}_{xx} = \frac{\partial (N_j \Delta u_{mxj})}{\partial x} = N_{j,x} \left[\int_{\xi_1}^{\xi_j} J_{1,1} \left(J_{1,1}^{-1} N_{i,\xi} u_i + J_{1,2}^{-1} N_{i,\eta} u_i \right) d\xi \Big|_{\eta=\eta_j} + \int_{\eta_1}^{\eta_j} J_{2,1} \left(J_{1,1}^{-1} N_{i,\xi} u_i + J_{1,2}^{-1} N_{i,\eta} u_i \right) d\eta \Big|_{\xi=\xi_j} \right] (40a)$$

$$\bar{\varepsilon}_{yy} = \frac{\partial (N_j \Delta \upsilon_{myj})}{\partial y} = N_{j,y} \left[\int_{\xi_1}^{\xi_j} J_{1,2} \left(J_{2,1}^{-1} N_{i,\xi} \upsilon_i + J_{2,2}^{-1} N_{i,\eta} \upsilon_i \right) d\xi \Big|_{\eta=\eta_j} + \int_{\eta_1}^{\eta_j} J_{2,2} \left(J_{2,1}^{-1} N_{i,\xi} \upsilon_i + J_{2,2}^{-1} N_{i,\eta} \upsilon_i \right) d\eta \Big|_{\xi=\xi_j} \right] (40b)$$

$$\bar{\gamma}_{xy} = \frac{\partial (N_j \Delta \bar{u}_{mxyj})}{\partial y} + \frac{\partial (N_j \Delta \upsilon_{mxyj})}{\partial x}$$

$$= N_{j,y} \left[\int_{\xi_1}^{\xi_j} J_{1,2} \left(J_{2,1}^{-1} N_{i,\xi} u_i + J_{2,2}^{-1} N_{i,\eta} u_i \right) d\xi \Big|_{\eta=\eta_j} + \int_{\eta_1}^{\eta_j} J_{2,2} \left(J_{2,1}^{-1} N_{i,\xi} u_i + J_{2,2}^{-1} N_{i,\eta} u_i \right) d\eta \Big|_{\xi=\xi_j} \right]$$

$$+ N_{j,x} \left[\int_{\xi_1}^{\xi_j} J_{1,1} \left(J_{1,1}^{-1} N_{i,\xi} \upsilon_i + J_{1,2}^{-1} N_{i,\eta} \upsilon_i \right) d\xi \Big|_{\eta=\eta_j} + \int_{\eta_1}^{\eta_j} J_{2,1} \left(J_{1,1}^{-1} N_{i,\xi} \upsilon_i + J_{1,2}^{-1} N_{i,\eta} \upsilon_i \right) d\eta \Big|_{\xi=\xi_j} \right] (40c)$$

Similarly, the discrete shear gaps are evaluated by integrating the shear strains over the element domain,

$$\bar{w}_{xzi} = \int_{\xi_1}^{\xi_i} \gamma_{xz} J_{1,1} d\xi \Big|_{\eta=\eta_i} + \int_{\eta_1}^{\eta_i} \gamma_{xz} J_{2,1} d\eta \Big|_{\xi=\xi_i} \qquad (41a)$$

$$\bar{w}_{yzi} = \int_{\xi_1}^{\xi_i} \gamma_{yz} J_{1,2} d\xi \Big|_{\eta=\eta_i} + \int_{\eta_1}^{\eta_i} \gamma_{yz} J_{2,2} d\eta \Big|_{\xi=\xi_i} \qquad (41b)$$

and the assumed shear strains are calculated as

$$\bar{\gamma}_{xz} = \frac{\partial(N_j\bar{w}_{xzj})}{\partial x} = N_{j,x}\left\{\int_{\xi_1}^{\xi_j} J_{1,1}\left[J_{1,1}^{-1}N_{i,\xi}w_i + J_{1,2}^{-1}\sum N_{i,\eta}w_i + N_i(r_{ix} - r_{ix})\right]d\xi\right|_{\eta=\eta_j}$$

$$+ \int_{\eta_1}^{\eta_j} J_{2,1}\left[J_{1,1}^{-1}N_{i,\xi}w_i + J_{1,2}^{-1}N_{i,\eta}w_i + N_i(r_{ix} - r_{ix})\right]d\eta\Big|_{\xi=\xi_j}\right\} \quad (42a)$$

$$\bar{\gamma}_{yz} = \frac{\partial(N_j\bar{w}_{yzj})}{\partial y} = N_{j,y}\left\{\int_{\xi_1}^{\xi_j} J_{1,2}\left[J_{2,1}^{-1}N_{i,\xi}w_i + J_{2,2}^{-1}N_{i,\eta}w_i + N_i(r_{iy} - r_{iy0})\right]d\xi\right|_{\eta=\eta_j}$$

$$+ \int_{\eta_1}^{\eta_j} J_{2,2}\left[J_{2,1}^{-1}N_{i,\xi}w_i + J_{2,2}^{-1}N_{i,\eta}w_i + N_i(r_{iy} - r_{iy0})\right]d\eta\Big|_{\xi=\xi_j}\right\} \quad (42b)$$

4 Transformation from local to global response

The internal force vector $\mathbf{f}_g$ of the curved quadrilateral shell element in the global coordinate system can be calculated from the internal force vector $\mathbf{f}$ in the local coordinate system:

$$\mathbf{f}_g = \mathbf{T}^{\mathrm{T}}\mathbf{f} \quad (43)$$

where the transformation matrix $\mathbf{T}$ can be calculated based upon the relationship between the local and global nodal variables

$$\mathbf{T} = \begin{bmatrix} \frac{\partial \mathbf{t}_1}{\partial \mathbf{d}_1^{\mathrm{T}}} & \mathbf{0} & & \frac{\partial \mathbf{t}_1}{\partial \mathbf{d}_6^{\mathrm{T}}} & \mathbf{0} \\ \frac{\partial \boldsymbol{\theta}_1}{\partial \mathbf{d}_1^{\mathrm{T}}} & \frac{\partial \boldsymbol{\theta}_1}{\partial \mathbf{n}_{g1}^{\mathrm{T}}} & \cdots & \frac{\partial \boldsymbol{\theta}_1}{\partial \mathbf{d}_6^{\mathrm{T}}} & \frac{\partial \boldsymbol{\theta}_1}{\partial \mathbf{n}_{g6}^{\mathrm{T}}} \\ \vdots & & \ddots & \vdots & \\ \frac{\partial \mathbf{t}_6}{\partial \mathbf{d}_1^{\mathrm{T}}} & \mathbf{0} & & \frac{\partial \mathbf{t}_6}{\partial \mathbf{d}_6^{\mathrm{T}}} & \mathbf{0} \\ \frac{\partial \boldsymbol{\theta}_6}{\partial \mathbf{d}_1^{\mathrm{T}}} & \frac{\partial \boldsymbol{\theta}_6}{\partial \mathbf{n}_{g1}^{\mathrm{T}}} & \cdots & \frac{\partial \boldsymbol{\theta}_6}{\partial \mathbf{d}_6^{\mathrm{T}}} & \frac{\partial \boldsymbol{\theta}_6}{\partial \mathbf{n}_{g6}^{\mathrm{T}}} \end{bmatrix} \quad (44)$$

The expressions of each sub-matrix in $\mathbf{T}$ is given in Appendix B.

The consistent element tangent stiffness matrix $\mathbf{k}_{Tg}$ in the global coordinate system is calculated by differentiating $\mathbf{f}_g$ with respect to the global nodal variable vector $\mathbf{u}_g$:

$$\mathbf{k}_{\mathrm{T}g} = \frac{\partial \mathbf{f}_g}{\partial \mathbf{u}_g^{\mathrm{T}}} = \mathbf{T}^{\mathrm{T}} \frac{\partial \mathbf{f}}{\partial \mathbf{u}_g^{\mathrm{T}}} + \frac{\partial \mathbf{T}^{\mathrm{T}}}{\partial \mathbf{u}_g^{\mathrm{T}}} \mathbf{f} = \mathbf{T}^{\mathrm{T}} \frac{\partial \mathbf{f}}{\partial \mathbf{u}_{\mathrm{L}}^{\mathrm{T}}} \mathbf{T} + \frac{\partial \mathbf{T}^{\mathrm{T}}}{\partial \mathbf{u}_g^{\mathrm{T}}} \mathbf{f} \Rightarrow$$

$$\mathbf{k}_{\mathrm{T}g} = \mathbf{T}^{\mathrm{T}} \mathbf{k}_{\mathrm{T}} \mathbf{T} + \frac{\partial \mathbf{T}^{\mathrm{T}}}{\partial \mathbf{u}_g^{\mathrm{T}}} \mathbf{f} \tag{45}$$

where

$$\frac{\partial \mathbf{T}}{\partial \mathbf{u}_g^{\mathrm{T}}} = \left[\frac{\partial^2 \mathrm{u}_{Li}}{\partial \mathrm{u}_{gj} \partial \mathrm{u}_{gk}} \right] = \begin{bmatrix} \frac{\partial^2 \mathbf{t}_1}{\partial \mathbf{d}_1^{\mathrm{T}} \partial \mathbf{u}_g^{\mathrm{T}}} & \mathbf{0} & & \frac{\partial^2 \mathbf{t}_1}{\partial \mathbf{d}_6^{\mathrm{T}} \partial \mathbf{u}_g^{\mathrm{T}}} & \mathbf{0} \\ \frac{\partial^2 \boldsymbol{\theta}_1}{\partial \mathbf{d}_1^{\mathrm{T}} \partial \mathbf{u}_g^{\mathrm{T}}} & \frac{\partial^2 \boldsymbol{\theta}_1}{\partial \mathbf{n}_{g1}^{\mathrm{T}} \partial \mathbf{u}_g^{\mathrm{T}}} & \cdots & \frac{\partial^2 \boldsymbol{\theta}_1}{\partial \mathbf{d}_6^{\mathrm{T}} \partial \mathbf{u}_g^{\mathrm{T}}} & \frac{\partial^2 \boldsymbol{\theta}_1}{\partial \mathbf{n}_{g6}^{\mathrm{T}} \partial \mathbf{u}_g^{\mathrm{T}}} \\ \vdots & & \ddots & \vdots & \\ \frac{\partial^2 \mathbf{t}_6}{\partial \mathbf{d}_1^{\mathrm{T}} \partial \mathbf{u}_g^{\mathrm{T}}} & \mathbf{0} & & \frac{\partial^2 \mathbf{t}_6}{\partial \mathbf{d}_6^{\mathrm{T}} \partial \mathbf{u}_g^{\mathrm{T}}} & \mathbf{0} \\ \frac{\partial^2 \boldsymbol{\theta}_6}{\partial \mathbf{d}_1^{\mathrm{T}} \partial \mathbf{u}_g^{\mathrm{T}}} & \frac{\partial^2 \boldsymbol{\theta}_6}{\partial \mathbf{n}_{g1}^{\mathrm{T}} \partial \mathbf{u}_g^{\mathrm{T}}} & \cdots & \frac{\partial^2 \boldsymbol{\theta}_6}{\partial \mathbf{d}_6^{\mathrm{T}} \partial \mathbf{u}_g^{\mathrm{T}}} & \frac{\partial^2 \boldsymbol{\theta}_6}{\partial \mathbf{n}_{g6}^{\mathrm{T}} \partial \mathbf{u}_g^{\mathrm{T}}} \end{bmatrix} \tag{46}$$

The detailed expressions of the sub-matrices in $\dfrac{\partial \mathbf{T}}{\partial \mathbf{u}_g^{\mathrm{T}}}$ are given in Appendix B. In Equation (45),

the term $\mathbf{T}^{\mathrm{T}} \mathbf{k}_T \mathbf{T}$ is obviously symmetric. In addition, owing to the commutativity of the global

nodal variables in the differentiation of Equation (46), the other term $\dfrac{\partial \mathbf{T}^{\mathrm{T}}}{\partial \mathbf{u}_g^{\mathrm{T}}} \mathbf{f}$ in Equation (45) is

also symmetric. Hence, the global consistent element tangent stiffness matrix shown in Equation

(45) is symmetric.

5 Numerical Examples

To demonstrate the computational performance of the present six-node co-rotational

triangular shell element (denoted as TRIA6), one smooth semi-cylindrical shell, one perforated

plate, and five folded/multi-shell problems involving large displacements and large rotations are

analyzed. An incremental-iterative procedure with generalized displacement control [44] is

employed in the analysis, and numerical results are compared to published reference solutions or

those obtained using engineering simulation software ANSYS [15,30-36] in order to verify the accuracy of the proposed TRIA6 element.

5.1 Pinching of a clamped semi-cylindrical shell

A semi-cylindrical shell is subjected to a vertical radial force at the middle point of the free circumferential edge, while the other circumferential edge is fully clamped. Along its two straight edges, the vertical translation and rotation around the corresponding straight edge are restrained. The material properties are $E = 2.0685 \times 10^{7}$, $\mu = 0.3$. The length and radius of the half cylinder are L=3.048 and R=1.016, respectively, and the thickness is a=0.03.
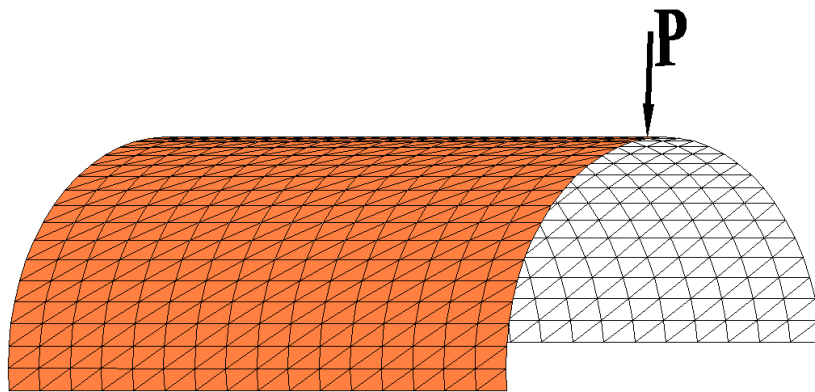
Fig. 2 A clamped semi-cylindrical shell subject to a point load at free end

The maximum load level is set to P=2000. Owing to symmetry, only a half of the semi-cylindrical shell (the colored zone in Figure 2) is analyzed using TRIA6 elements with two meshes of 33×33 and 65×65 nodes, respectively. Converged solution is obtained with 25 loading steps, and there are 5~6 iterations in each loading step with a tolerance of err=1×10⁻⁶(referred to [25], Eq.67).The load-deflection curves at the loading point are depicted in Fig.3. For comparison, Fig. 3 also provides the results from Brank et. al [30] and Parisch [31] using four-node quadrilateral degenerated solid shell elements with a mesh of 17×17 nodes, Sze et. al [32] using S4R (four-node quadrilateral) elements of the finite element program ABAQUS with a mesh of 33×33 nodes, and Xiong et. al [33] using seven-node triangular solid-shell elements with a mesh

of 65×65 nodes. It is shown that the results from TRIA6 elements with 33×33 and 65×65 meshes

agree very well with the reference solutions.
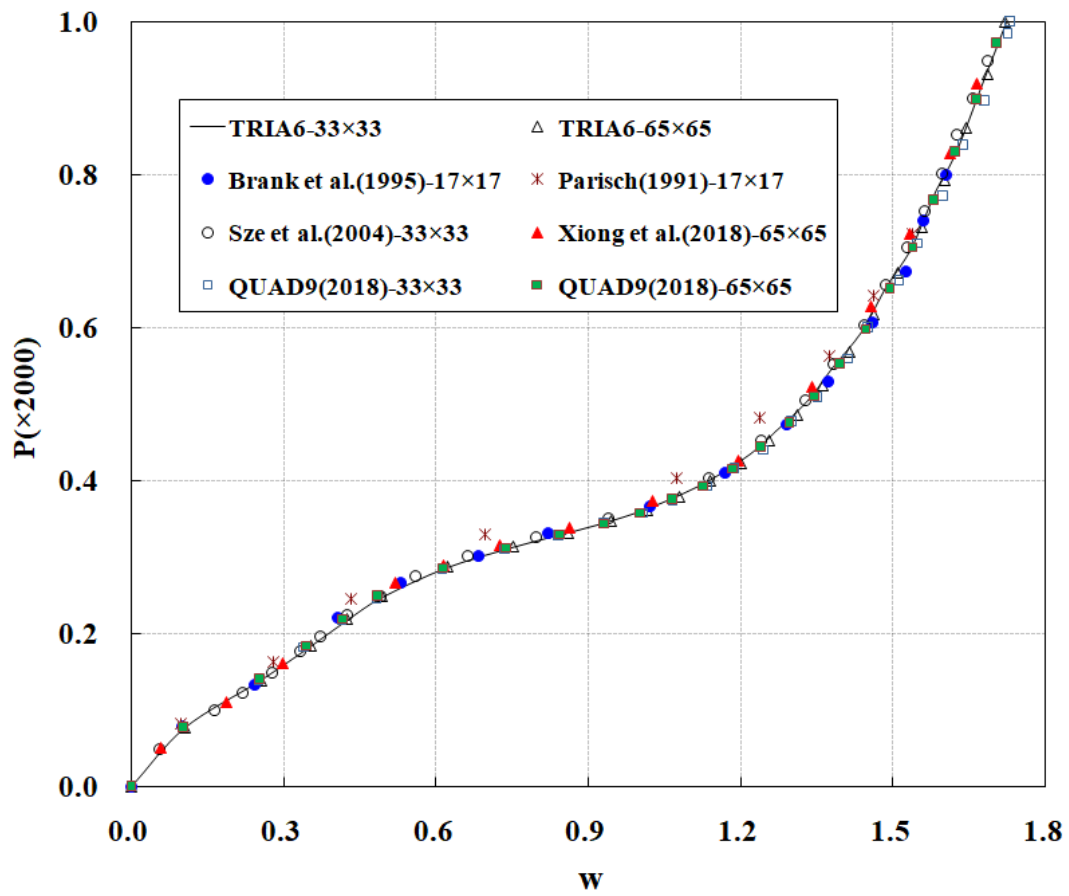
Fig. 3 Load deflection curves at the loading point of
clamped semi-cylindrical shell

Fig. 4 shows the deformed shape of the clamped semi-cylindrical shell using TRIA6 elements

with the mesh of 33×33 nodes at the maximum load level P=2000. As can be seen, TRIA6

effectively captures the large displacement and large rotation of the smooth shell structure.
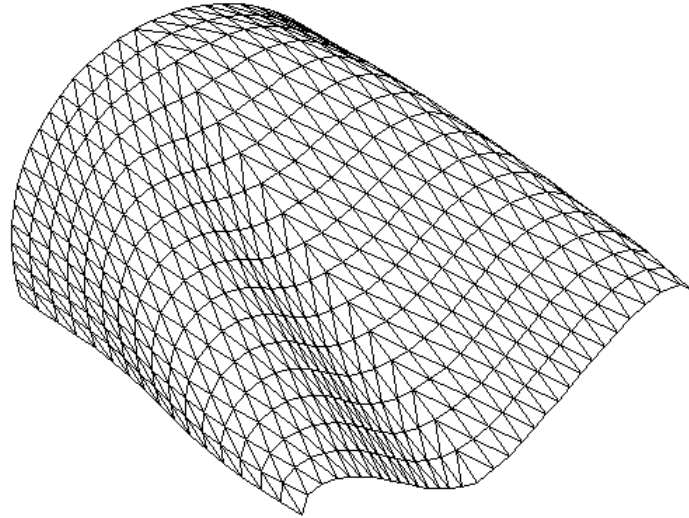
Fig. 4 Deformed shape of the clamped semi-cylindrical shell at the load level P=2000

5.2 A clamped perforated plate under distributed pressure

A plate with 7 holes is clamped along its left edge, and the plate surface is subjected to uniform pressure q=0.1N/mm^2. The material properties are Young's modulus E=210,000MPa and Poisson ratio μ=0.3, respectively. The plate thickness is 0.1mm, and the radius of each hole is 1mm, and other geometrical parameters are presented in Fig.5a, where finite element meshes with 116, 280, 406 and 706 TRIA6 elements are also depicted, respectively. For complex shell geometries, it is non-trivial to generate high-quality meshes using quadrilateral finite elements (e.g., the co-rotational element in [25]). On the other hand, the present triangular co-rotational finite element allows the employment of efficient automatic mesh generation techniques, making it advantageous in modeling shell structures with complex geometries.
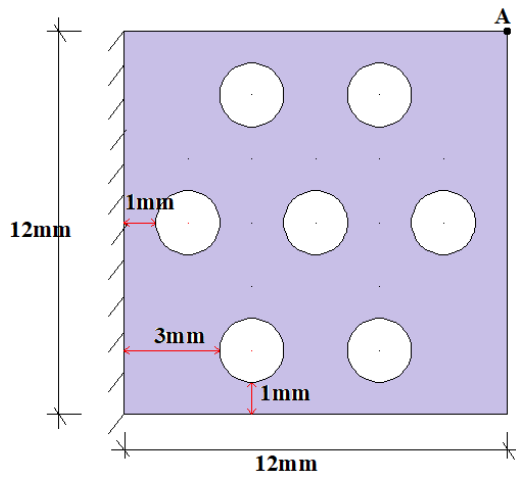
(a) Geometry of the clamped perforated plate
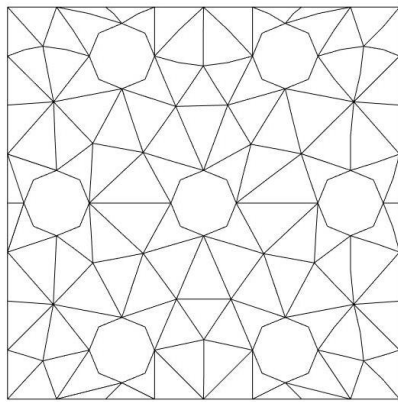
(b) Mesh with 116 elements and 286 nodes
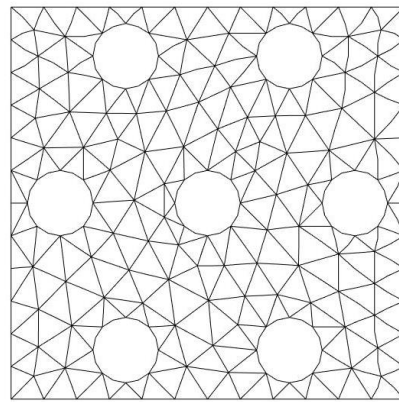
(c) Mesh with 280 elements and 658 nodes
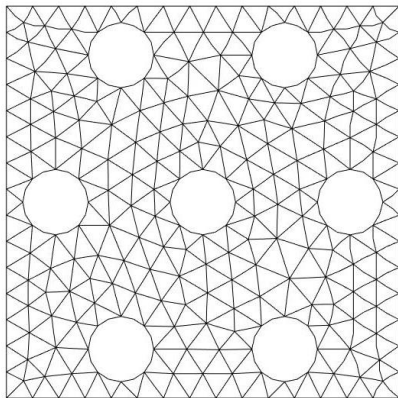
(d) Mesh with 406 elements and 922 nodes
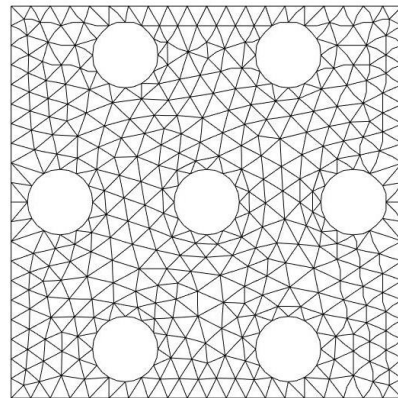
(e) Mesh with 706 elements and 1570 nodes

Fig.5 Geometry and finite element meshes for the clamped perforated plate

The load-deflection curves for the corner point A are obtained by using TRIA6 elements, and the results are plotted in Fig. 6, where, for comparison, we have also plotted the results obtained by using Shell 281 elements of ANSYS [34] based on the same six-node triangular element discretization. As can be seen, the results of TRIA6 element agree quite well with the Shell 281 element of ANSYS, and very accurate solution is obtained by using 280 TRIA6 elements with 18 loading steps, and 3~5 iterations in each loading step, the tolerance is err=1×10^{-6} (referred to [25], Eq.67). Figure 7 depicts the total vertical displacement at Point A versus different levels of mesh discretization, which clearly shows that TRIA6 achieves good convergence in the nonlinear large deformation analysis.
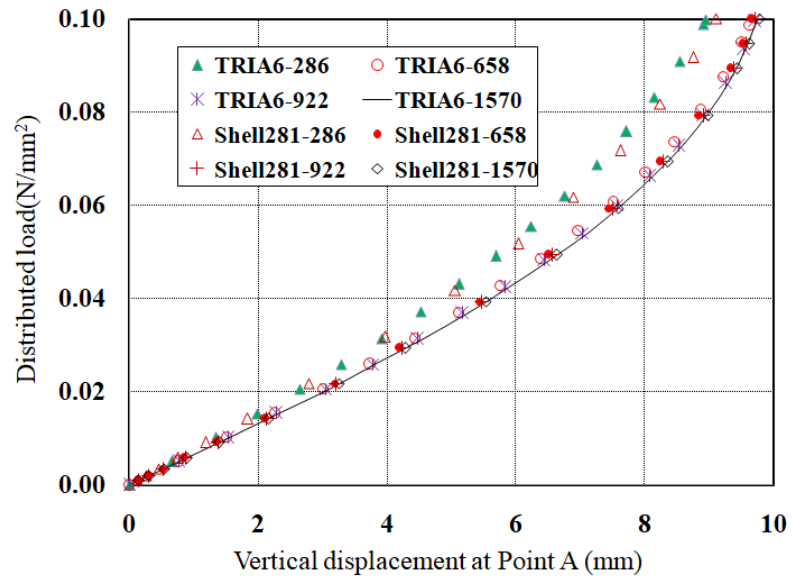
Fig.6 Load-deflection curves at Point A of the clamped perforated plate
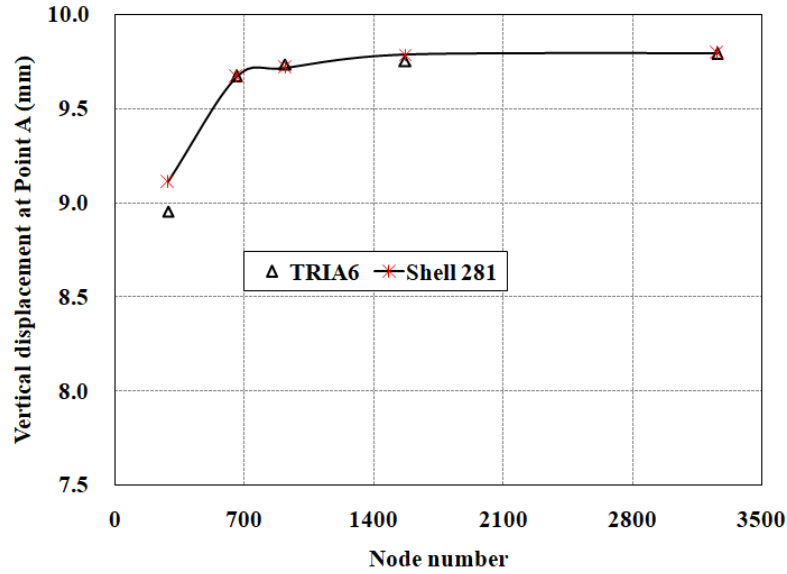
Fig.7 Convergence plot of Tria6 element

Table 1 presents the values of the total vertical displacement at Point A of the clamped perforated plate under distributed pressure $q=0.1N/mm^2$, they are obtained respectively by using 4 kinds of element meshes of TRIA6 and Shell 281 elements. In calculating the relative errors, the vertical displacement solution 9.79mm obtained from a highly refined mesh (1518 elements and 3262 nodes) of ANSYS's Shell 281 elements is taken as the reference solution. As shown in this table, the proposed TRIA6 element converges well upon mesh refinement for the nonlinear shell structural analysis involving large rotations.

Table 1. Vertical displacement at Point A of the perforated plate

Element type	TRIA6 element				Shell 281 element			
Element number	116	280	406	706	116	280	406	706
Node number	286	658	922	1570	286	658	922	1570
vertical displacement (mm)	8.95	9.67	9.74	9.75	9.11	9.67	9.72	9.79
Relative errors	-8.60%	-1.26%	-0.60%	-0.44%	-6.98%	-1.28%	-0.80%	-0.08%

In Figure 8, the initial and the final deformed shapes of the clamped perforated plate modeled by 280 TRIA6 elements are plotted. It is shown that large displacements and large rotations occur

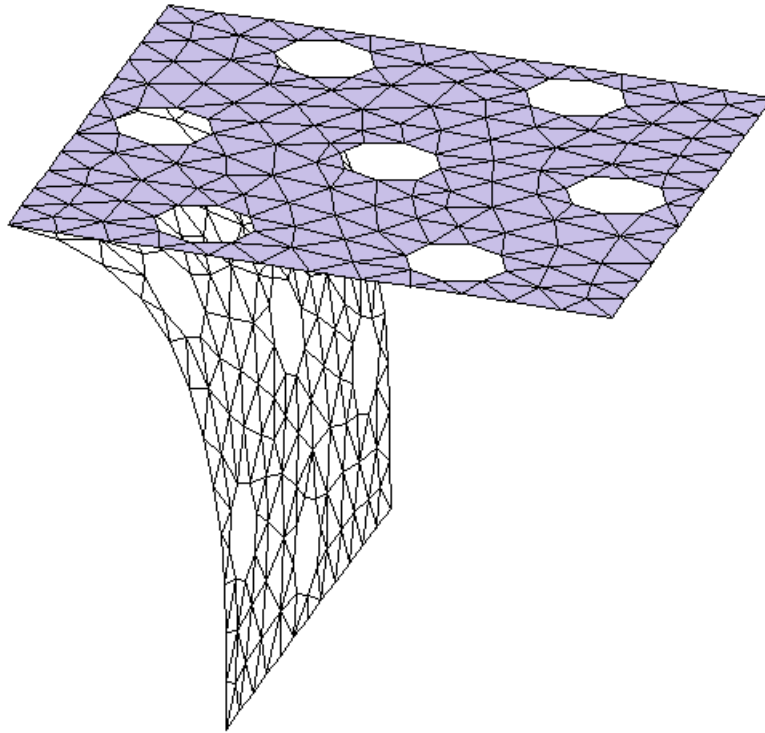in the structural deformation process.

Fig.8 Deformed shape of the clamped plate with 7 holes subject to distributed load 0.1N/mm^2

5.3 A Right-Angled Cantilever Plate subject to Distributed Tip Forces/Moments

Chroscielewski et al. [35] analyzed a right-angled cantilever plate, which is clamped at one end and subjected to distributed forces or distributed moments at the other end Figs.9a,b. The adopted material and geometric properties include Young's modulus $E = 3 \times 10^7$, Poisson's ratio μ=0.0, length L=12, width b=3, and thickness a=0.03.

a) Distributed tip force   b) Distributed tip moment
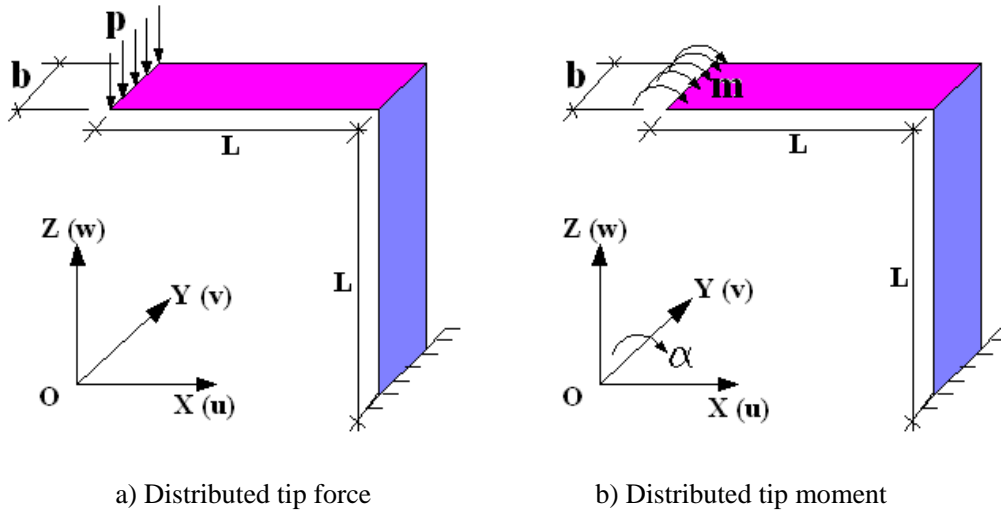
Fig.9 A right-angled cantilever plate structure subject to distributed tip forces/moments

In the present study, two loading cases of distributed forces and moments are analyzed using 49×5 node meshes of TRIA6 elements. The obtained load-displacement curves are depicted in Fig. 10 and Fig. 11, respectively. For comparison, the results using 25×3 node meshes of "Shell 181" elements from the finite element program ANSYS 18.0 [36] are also plotted as reference solutions, where Shell 181 refers to a four-node quadrilateral shell element with six DOFs per node, including a drilling rotation. As can be seen, the results of the present TRIA6 element formulation agree quite well with the reference solutions.
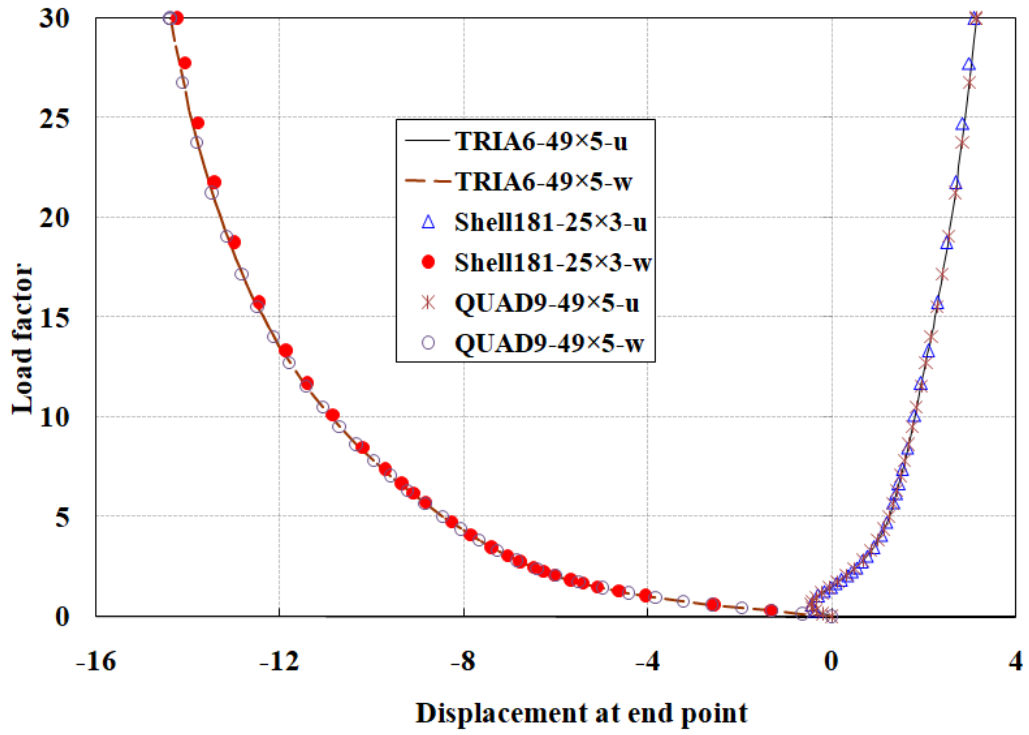
Fig. 10 Load-displacement curves of right-angled cantilever plate subject to distributed tip force
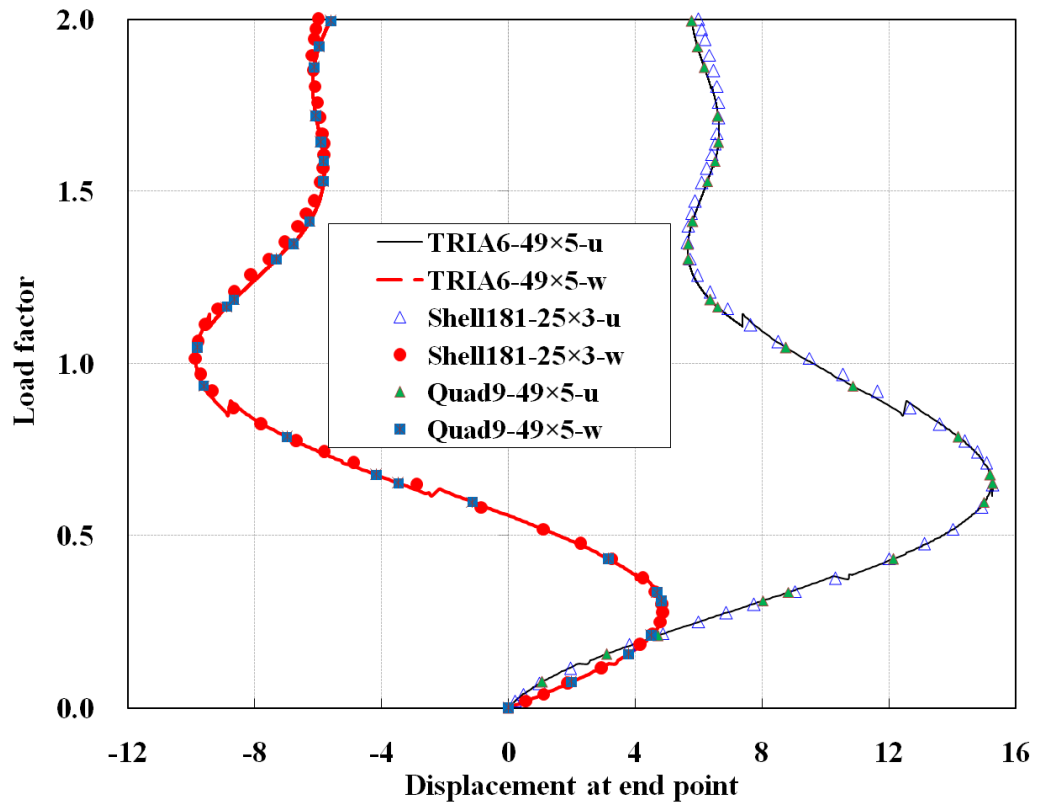
Fig.11 Load-displacement curves of right-angle cantilever plate subject to distributed tip moment

The deformed shapes of the cantilever plate subject to distributed tip forces and tip moments are plotted in Figs. 12a and 12b, respectively, where large displacements and large rotations can be clearly observed.
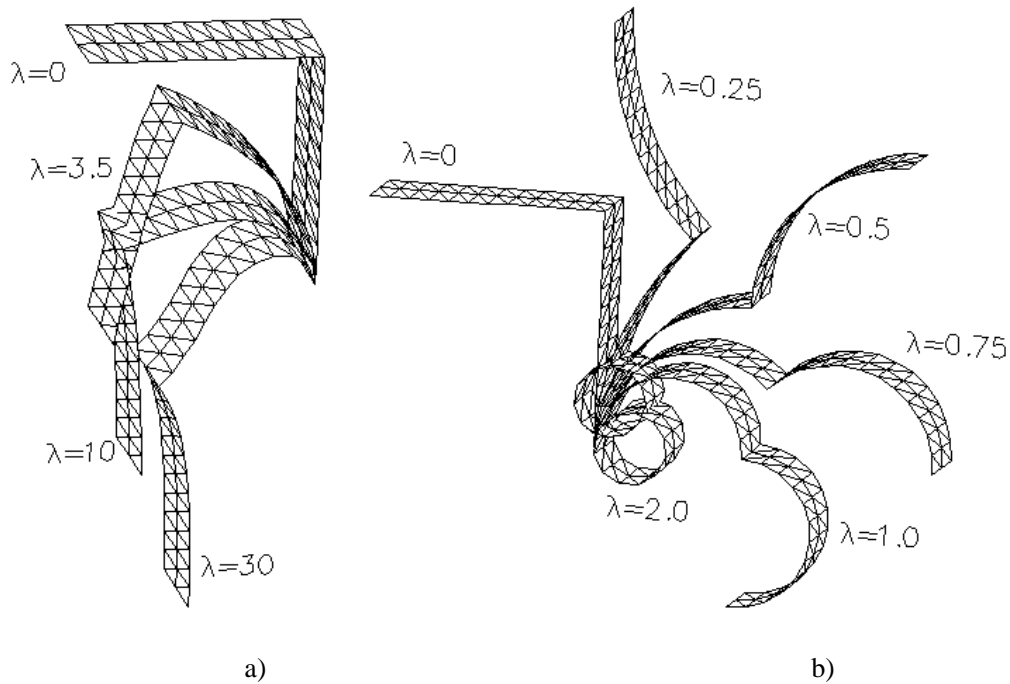

a)   b)

Fig.12 Deformed shapes of right-angle cantilever under different magnitudes of

distributed tip force and moment

5.4 Cantilever Sickle Shell subject to a Lateral Tip Force

A cantilever sickle shell is subjected to a lateral force at the free end (Fig. 13). The sickle shell has a radius R=5, length L=10, width B=1,and thickness a=0.01. The adopted material parameters are Young's modulus $E = 3 \times 10^7$ and Poisson's ratio $\mu = 0.3$.
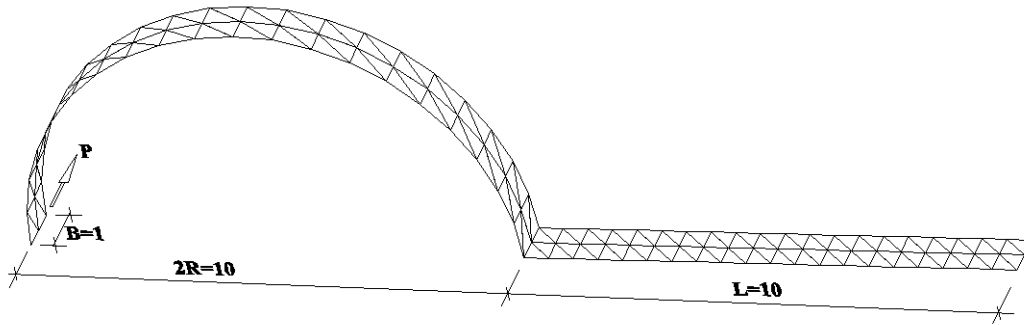
Fig.13 A cantileversickle shell subject to a lateral tip force

The sickle shell is discretized using 81×5 node meshes of TRIA6 elements, and the obtained load-deflection curves at the midpoint of the free end edge are plotted in Fig. 14. The results from Chroscielewski et al. [35] using 41×5 node meshes of SEMe9 elements (nine-node stress-resultant semi-mixed shell element) and 41×5 node meshes of SELe9 elements (nine-node degenerated shell element with six DOFs per node), including a drilling rotation are also given in this figure. The resultsusing 81×5 TRIA6 elements compare favourably with those using 41×5 node meshes of SELe9 elements.
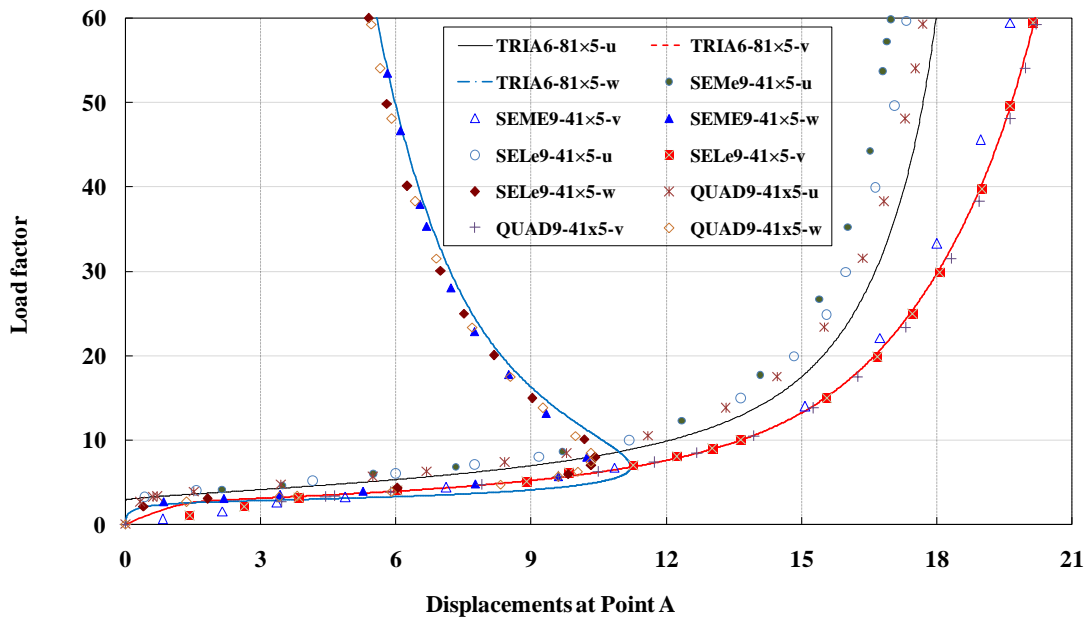

Fig.14 Load-displacement curves of cantilever sickle shell subject to a lateral tip force

The deformed shapes of the sickle shell at different lateral tip force levels are shown in Fig. 15.
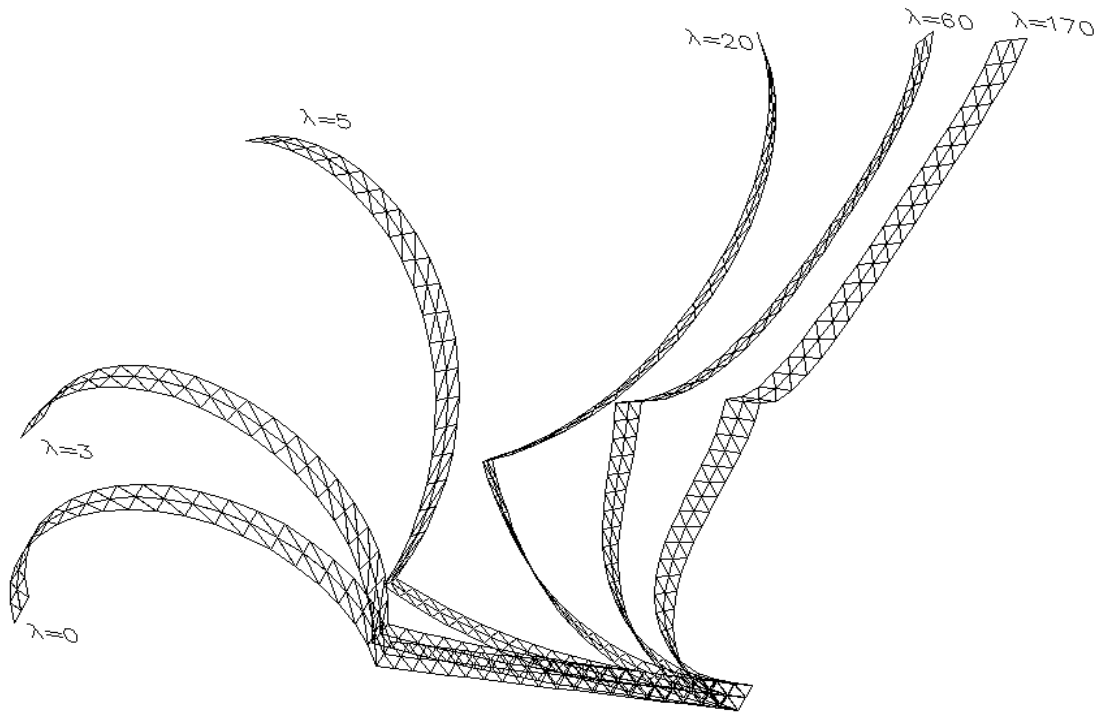
28

Fig.15 Deformed shapes of cantilever sickle shell at different levels of the tip force

5.5A cantilever I-beam subjected to a transverse tip force

Fig. 16 depicts a cantilever I-beam subjected to a transverse tip force lying in the X-Z plane. The concentrated force is applied at the center point on the cross section of the free end. The beam geometry is characterized by length L=4800mm, flange width b=300mm, web height h_w=300mm, thickness for both flange and web a=25mm. The adopted material properties are Young's modulus $E = 2 \times 10^5 \ N/mm^2$, and Poison's ratio $\mu = 0.3$.

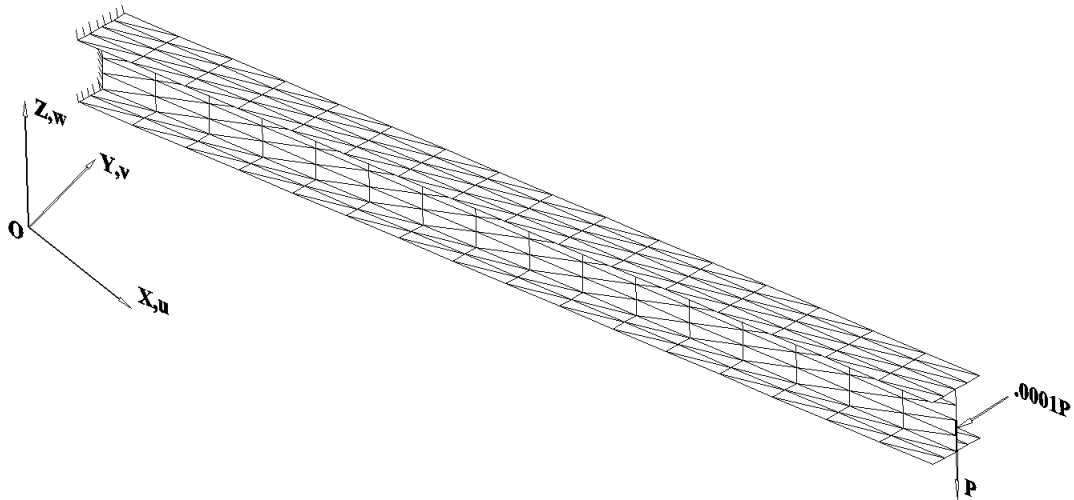**Fig.** 16 Cantilever I-beam subjected to a transverse tip force

A mesh of 25×33 node meshes of TRIA6 elements is used to model this I-beam. To determine the critical load, a perturbation tip force with magnitude l/1000th of the transverse tip force is applied at the centre of the free end in the Y-Z plane until the beam reaches a critical state. Once instability occurs, i.e., when the beam begins to bend sideways, this perturbation load is removed. The load-displacement curves at the centre of the I-beam are plotted in Fig. 17. For comparison, the results from Chroscielewski et al. [35] using 13×17 node meshes of CAMe9 elements (Lagrange family of nine-node shell elements with drilling rotations), 7×9 and 13×17 node meshes of SEMe4 elements, and 13×17 SEMe9 elements and Li et al.[25] using 13×17 node meshes of QUAD9 elements are also presented in this figure. The solutions using 25×33 TRIA6 elements agree very well with those using 13×17 node meshes of SEMe9 elements and QUAD9 elements, respectively.
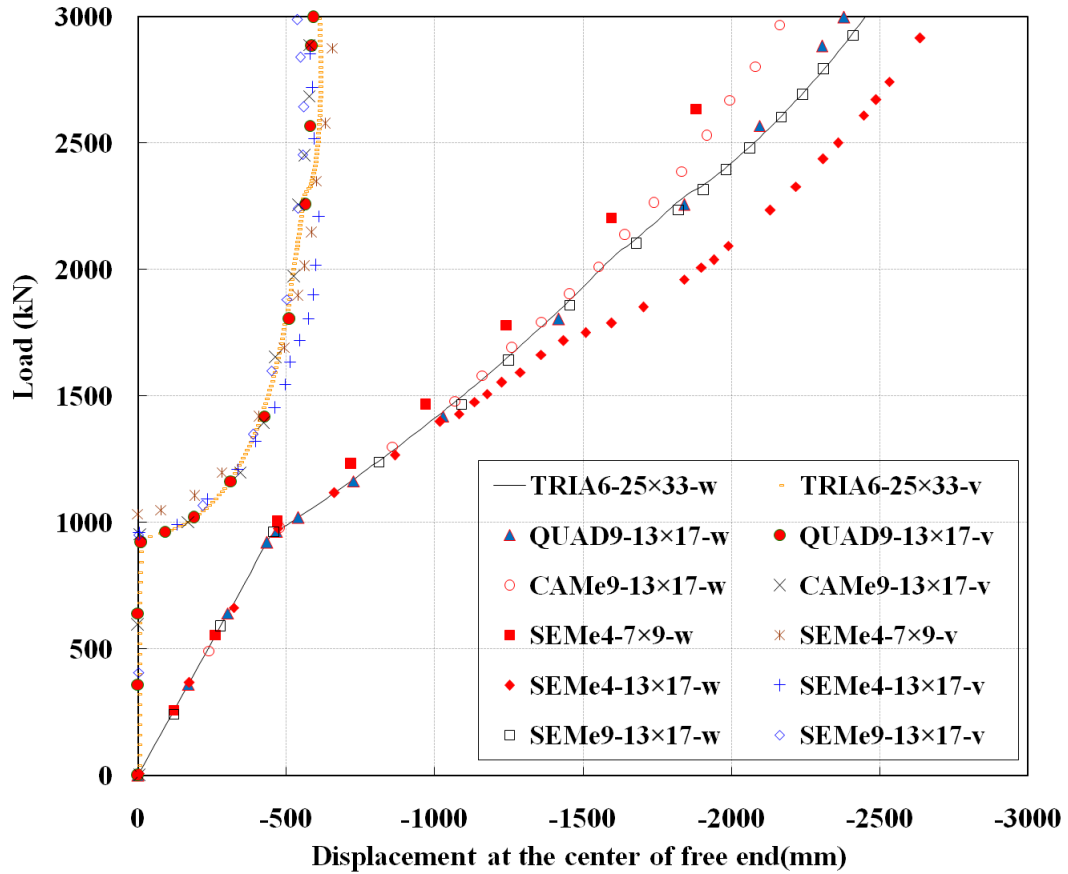
Fig. 17 Load-displacement curves of cantilever I-beam subject to a transverse tip force

The deformed shape of the I-beam under the force of magnitude $P = \lambda P_{ref}$ with $\lambda = 3297$

and $P_{ref} = 1000N$, are plotted in Fig. 18 together with its undeformed shape. As can be seen, the

large displacement and large rotation of the non-smooth shell structure are effectively captured by
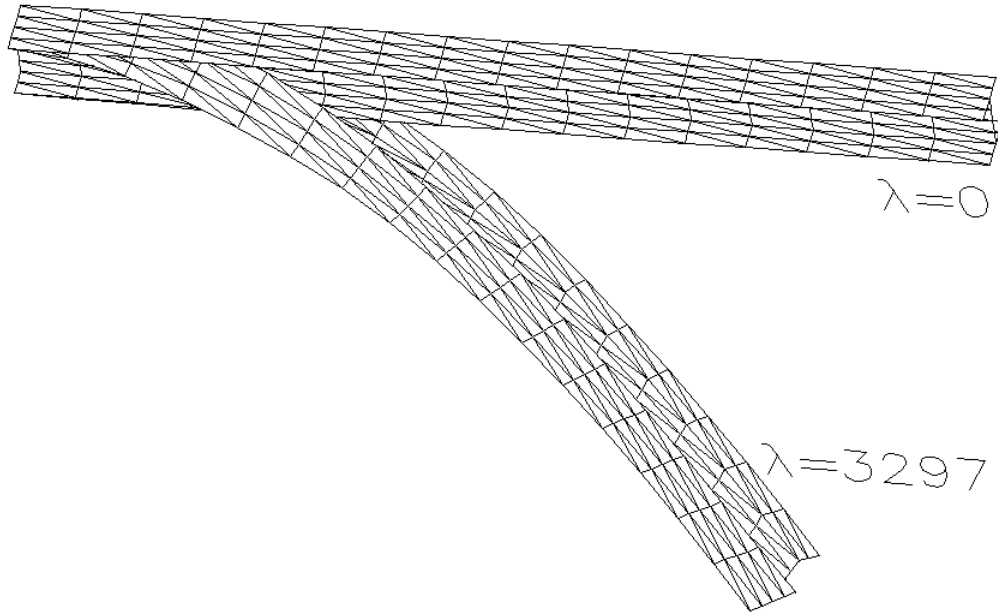
the proposed TRIA6 element.

Fig. 18 Deformed shapes of cantilever I-beam subject to transverse tip force

5.6 Intersecting-Plate Structure

A structure consisting of three intersecting flat plates is subjected to six concentrated forces at six different points, as shown in Fig. 19.The boundary conditions and external loads are selected to bend the front plate and induce torsional deflection of the middle plate. Consequently, the induced torque must be supported by the clamped plate. The geometric dimensions of the intersecting plates are presented in Fig. 19. All three plates have the same thickness $a = 0.02$. The material properties are Young's modulus $E = 2 \times 10^7$ and Poisson's ratio $\mu = 0.25$. All external loads are controlled by the same loading factor with a reference load $P_{ref} = 2$ in a nonlinear incremental-iterative solution procedure.
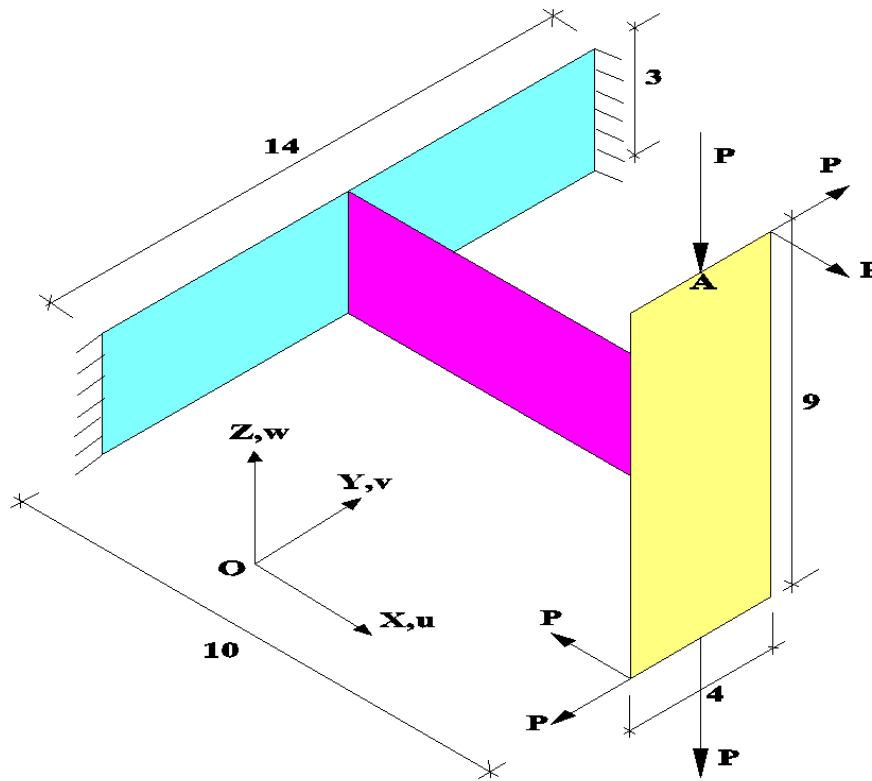
Fig.19 Intersecting plates subject to six concentrated forces

317×49 node meshes of TRIA6 elements are used to model the intersecting-plate structure. The obtained load-displacement curves at Point A are plotted in Fig. 20. The results obtained using respectively 317×49 node meshes of QUAD9 elements [25], 313×37 and 337×73 node meshes of EANS4 elements (4-node shell element with drilling rotations) [12] are also reported in this figure for comparison. The results using 317×49 node meshes of TRIA6 elements agree well with those using 317×49 node meshes of QUAD9 elements [25] and 337×73 node meshes of EANS4 elements [12].

Fig. 20 Load-displacement curves at Point A of intersecting-plate structure subject to six
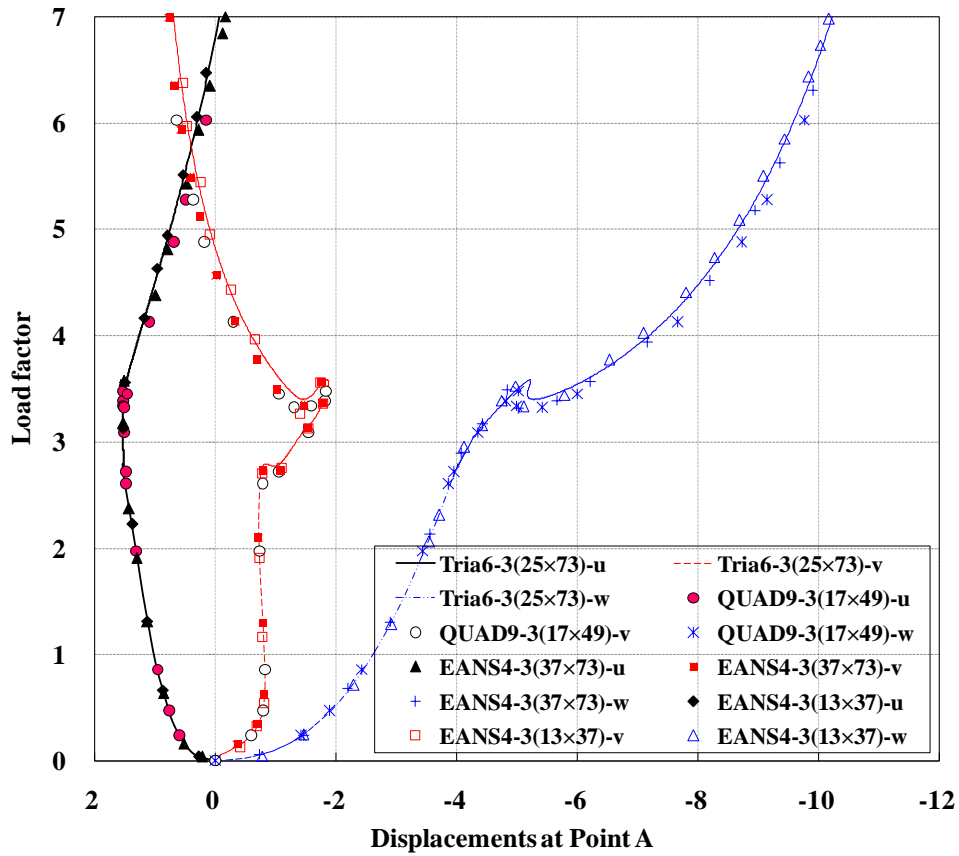
concentrated forces

The initial and deformed shapes of the intersecting-plate structure at the loading magnitude
$\lambda = 7$ are given in Fig. 21. The large deformation of the intersecting-plate structure is effectively
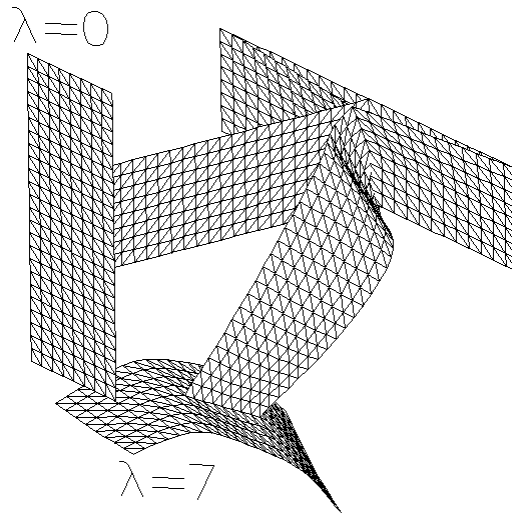captured by the proposed TRIA6 element.

Fig. 21 Initial and deformed shapes of intersecting-plate structure

6 Conclusions

A six-node co-rotational curved triangular shell element formulation for modeling smooth, folded and multi-shell structures undergoing large displacements and large rotations is presented. Different from other co-rotational shell element formulations, additive and commutative vectorial rotational variables are employed, resulting in symmetric consistent tangent stiffness matrices in both local and global coordinate systems. These vectorial rotational variables are components of the shell directors or orientation vectors, which are additive and commutative polar/proper vectors, instead of non-additive and non-commutative rotation axial/pseudo vectors. In addition, the membrane strains and out-of-plane shear strains are replaced with assumed strains based upon the modified discrete strain gap to achieve a locking-free six-node curved triangular shell element. The reliability and computational accuracy of the present shell formulation are demonstrated in solving several smooth, folded and multi-shell problems involving large displacements and large rotations. We note that, in terms of computational accuracy, the nine-node quadrilateral shell element in [25] shows better performance over the present co-rotational six-node triangular element. Nevertheless, when shell structures with complex geometries are encountered, such as

35

the perforated plate/shell structures, the present shell finite element in conjunction with automatic triangular mesh generation techniques will be very attractive for practical engineering applications. In addition, the present study adopts the classical shell model's zero thickness stress assumption, which restricts the element to specific class of material laws. Numerical procedures to incorporate thickness strains [45] in the proposed co-rotational shell element will be investigated in order to employ finite strain 3D constitutive models in nonlinear shell structural analysis.

APPENDIX A: Various Derivatives of Strains with respect to Local Nodal Variables

The first-order derivatives of membrane strains with respect to local nodal variables lead to the following gradient matrix

$$\mathbf{B}_m = \begin{bmatrix} \mathbf{B}_{m1} & \mathbf{0} & ... & \mathbf{B}_{m6} & \mathbf{0} \end{bmatrix} \qquad\text{(A-1a)}$$

in which the sub-matrix is expressed as

$$\mathbf{B}_{mi} = \begin{bmatrix} N_{i,x} & 0 & 0 \\ 0 & N_{i,y} & 0 \\ N_{i,y} & N_{i,x} & 0 \end{bmatrix} i{=}1,2,\dots,6 \qquad\text{(A-1b)}$$

Following the Equation (33a,b), the shape function derivatives can be expressed as follows

$$N_{i,x} = J_{11}^{-1} N_{i,\xi} + J_{12}^{-1} N_{i,\eta} \qquad\text{(A-2a)}$$

$$N_{i,y} = J_{21}^{-1} N_{i,\xi} + J_{22}^{-1} N_{i,\eta} \qquad\text{(A-2b)}$$

where $J_{jk}^{-1}(j,k=1,2)$ is the component of inverse Jacobian matrix at *jth* row and *kth* column; $N_{i,\xi}$ and $N_{i,\eta}$ are respectively the first-order derivative of the shape function N_i with respect to ξ and η.

The first-order derivatives of shear strains with respect to local nodal variables lead to the following gradient matrix:

$$B_\gamma = \begin{bmatrix} B_{r1} & B_{\gamma2} & ... & B_{r11} & B_{r12} \end{bmatrix} \qquad\text{(A-3a)}$$

in which

$$\mathbf{B}_{\gamma(2i-1)} = \begin{bmatrix} 0 & 0 & N_{i,x} \\ 0 & 0 & N_{i,y} \end{bmatrix} \qquad i=1,2,\ldots,6 \qquad\qquad (A\text{-}3b)$$

$$\mathbf{B}_{\gamma(2i)} = \begin{bmatrix} N_i & 0 \\ 0 & N_i \end{bmatrix} \qquad i=1,2,\ldots,6 \qquad\qquad (A\text{-}3c)$$

The first-order derivatives of bending strains with respect to local nodal variables lead to the following gradient matrix:

$$\mathbf{B}_b = \begin{bmatrix} \mathbf{0} & \mathbf{B}_{b1} & \ldots & \mathbf{0} & \mathbf{B}_{b6} \end{bmatrix} \qquad\qquad (A\text{-}4a)$$

in which

$$\mathbf{B}_{bi} = \begin{bmatrix} N_{i,x} & 0 \\ 0 & N_{i,y} \\ N_{i,y} & N_{i,x} \end{bmatrix} \qquad i=1,2,\ldots,6 \qquad\qquad (A\text{-}4b)$$

The first-order derivatives of assumed membrane strains with respect to local nodal variables lead to the following gradient matrix

$$\overline{\mathbf{B}}_m = \begin{bmatrix} \overline{\mathbf{B}}_{m1} & \mathbf{0} & \ldots & \overline{\mathbf{B}}_{m6} & \mathbf{0} \end{bmatrix} \qquad\qquad (A\text{-}5a)$$

in which the sub-matrix is expressed as

$$\bar{B}_{mi} = \begin{bmatrix} N_{j,x}\left(\int_{\xi_1}^{\xi_j} J_{1,1} N_{i,x} d\xi \Big|_{\eta=\eta_j} + \int_{\eta_1}^{\eta_j} J_{2,1} N_{i,x} d\eta \Big|_{\xi=\xi_j} \right) & 0 & 0 \\ 0 & N_{j,y}\left(\int_{\xi_1}^{\xi_j} J_{1,2} N_{i,y} d\xi \Big|_{\eta=\eta_j} + \int_{\eta_1}^{\eta_j} J_{2,2} N_{i,y} d\eta \Big|_{\xi=\xi_j} \right) & 0 \\ N_{j,y}\left(\int_{\xi_1}^{\xi_j} J_{1,2} N_{i,y} d\xi \Big|_{\eta=\eta_j} + \int_{\eta_1}^{\eta_j} J_{2,2} N_{i,y} d\eta \Big|_{\xi=\xi_j} \right) & N_{j,x}\left(\int_{\xi_1}^{\xi_j} J_{1,1} N_{i,x} d\xi \Big|_{\eta=\eta_j} + \int_{\eta_1}^{\eta_j} J_{2,1} N_{i,x} d\eta \Big|_{\xi=\xi_j} \right) & 0 \end{bmatrix}$$

$$(A\text{-}5b)$$

The first-order derivatives of assumed shear strains with respect to local nodal variables lead to the following gradient matrix

$$\overline{\mathbf{B}}_\gamma = \begin{bmatrix} \overline{\mathbf{B}}_{r1} & \overline{\mathbf{B}}_{\gamma 2} & \ldots & \overline{\mathbf{B}}_{r11} & \overline{\mathbf{B}}_{r12} \end{bmatrix} \qquad\qquad (A\text{-}6a)$$

in which the sub-matrices are expressed as

$$\bar{B}_{\gamma(2i-1)} = \begin{bmatrix} 0 & 0 & N_{j,x}\left(\int_{\xi_1}^{\xi_j} J_{1,1}N_{i,x}d\xi\Big|_{\eta=\eta_j} + \int_{\eta_1}^{\eta_j} J_{2,1}N_{i,x}d\eta\Big|_{\xi=\xi_j}\right) \\ 0 & 0 & N_{j,y}\left(\int_{\xi_1}^{\xi_j} J_{1,2}N_{i,y}d\xi\Big|_{\eta=\eta_j} + \int_{\eta_1}^{\eta_j} J_{2,2}N_{i,y}d\eta\Big|_{\xi=\xi_j}\right) \end{bmatrix}$$
(A-6b)

$$\overline{\mathbf{B}}_{\gamma(2i)} = \begin{bmatrix} N_{j,x}\left(\int_{\xi_1}^{\xi_j} J_{1,1}N_i d\xi\Big|_{\eta=\eta_j} + \int_{\eta_1}^{\eta_j} J_{2,1}N_i d\eta\Big|_{\xi=\xi_j}\right) & 0 \\ 0 & N_{j,y}\left(\int_{\xi_1}^{\xi_j} J_{1,2}N_i d\xi\Big|_{\eta=\eta_j} + \int_{\eta_1}^{\eta_j} J_{2,2}N_i d\eta\Big|_{\xi=\xi_j}\right) \end{bmatrix}$$
(A-6c)

APPENDIX B: Sub-matrices of Transformation Matrix T and Its Derivatives with Respect to Global Nodal Variables

The sub-matrices of the transformation matrix $\mathbf{T}$ can be expressed as

$$\frac{\partial \mathbf{t}_k}{\partial \mathbf{d}_l^{\mathrm{T}}} = \frac{\partial \mathbf{R}}{\partial \mathbf{d}_l^{\mathrm{T}}}(\mathbf{d}_k + \mathbf{v}_{k0}) + \mathbf{R}\delta_{kl}\mathbf{I} = \left(\frac{\partial}{\partial \mathbf{d}_l^{\mathrm{T}}}\begin{bmatrix} \mathbf{e}_x^{\mathrm{T}} \\ \mathbf{e}_y^{\mathrm{T}} \\ \mathbf{e}_z^{\mathrm{T}} \end{bmatrix}\right)(\mathbf{d}_k + \mathbf{v}_{k0}) + \mathbf{R}\delta_{kl}\mathbf{I}$$
(B-1)

If Node k is within a piece of smooth shell or away from intersections of non-smooth shells, two vectorial rotational variables are employed in the global coordinate system. Hence, the corresponding sub-matrices of $\mathbf{T}$ are evaluated as follows

$$\frac{\partial \boldsymbol{\theta}_k}{\partial \mathbf{d}_l^{\mathrm{T}}} = \frac{\partial \mathbf{R}_h}{\partial \mathbf{d}_l^{\mathrm{T}}}\mathbf{p}_k = \left(\frac{\partial}{\partial \mathbf{d}_l^{\mathrm{T}}}\begin{bmatrix} \mathbf{e}_x^{\mathrm{T}} \\ \mathbf{e}_y^{\mathrm{T}} \end{bmatrix}\right)\mathbf{p}_k$$
(B-2)

$$\frac{\partial \boldsymbol{\theta}_k}{\partial \mathbf{n}_{gl}^{\mathrm{T}}} = \mathbf{R}_h \delta_{kl}\frac{\partial \mathbf{p}_k}{\partial \mathbf{n}_{gl}^{\mathrm{T}}} = \begin{bmatrix} \mathbf{e}_x^{\mathrm{T}} \\ \mathbf{e}_y^{\mathrm{T}} \end{bmatrix}\delta_{kl}\frac{\partial \mathbf{p}_k}{\partial \mathbf{n}_{gl}^{\mathrm{T}}}$$
(B-3)

$$\frac{\partial \mathbf{e}_x}{\partial \mathbf{d}_l^{\mathrm{T}}} = \left(\frac{\mathbf{I}}{|\mathbf{v}_{12}|} - \frac{\mathbf{v}_{12}\otimes\mathbf{v}_{12}}{|\mathbf{v}_{12}|^3}\right)\frac{\partial \mathbf{v}_{12}}{\partial \mathbf{d}_l^{\mathrm{T}}}$$
(B-4)

$$\frac{\partial \mathbf{e}_z}{\partial \mathbf{d}_l^{\mathrm{T}}} = \left[\frac{\mathbf{I}}{|\mathbf{v}_{12}\times\mathbf{v}_{13}|} - \frac{(\mathbf{v}_{12}\times\mathbf{v}_{13})\otimes(\mathbf{v}_{12}\times\mathbf{v}_{13})}{|\mathbf{v}_{12}\times\mathbf{v}_{13}|^3}\right]\left(\frac{\partial \mathbf{v}_{12}}{\partial \mathbf{d}_l^{\mathrm{T}}}\times\mathbf{v}_{13} + \mathbf{v}_{12}\times\frac{\partial \mathbf{v}_{13}}{\partial \mathbf{d}_l^{\mathrm{T}}}\right)$$
(B-5)

$$\frac{\partial \mathbf{e}_y}{\partial \mathbf{d}_l^{\mathrm{T}}} = \frac{\partial \mathbf{e}_z}{\partial \mathbf{d}_l^{\mathrm{T}}}\times\mathbf{e}_x + \mathbf{e}_z\times\frac{\partial \mathbf{e}_x}{\partial \mathbf{d}_l^{\mathrm{T}}}$$
(B-6)

In Equations (B-4)-(B-5), $\dfrac{\partial \mathbf{v}_{12}}{\partial \mathbf{d}_l^{\mathrm{T}}} = -\mathbf{I}$, $l=1$; $\dfrac{\partial \mathbf{v}_{12}}{\partial \mathbf{d}_l^{\mathrm{T}}} = \mathbf{I}$, $l=2$; $\dfrac{\partial \mathbf{v}_{12}}{\partial \mathbf{d}_l^{\mathrm{T}}} = 0$, $l = 3,4,5$ or 6;

$\dfrac{\partial \mathbf{v}_{13}}{\partial \mathbf{d}_l^{\mathrm{T}}} = -\mathbf{I}$, $l=1$; $\dfrac{\partial \mathbf{v}_{13}}{\partial \mathbf{d}_l^{\mathrm{T}}} = \mathbf{I}$, $l=3$; $\dfrac{\partial \mathbf{v}_{13}}{\partial \mathbf{d}_l^{\mathrm{T}}} = 0$, $l = 2,4,5$ or 6.

$$\frac{\partial \mathbf{p}_k}{\partial \mathbf{n}_{gk}^{\mathrm{T}}} = \begin{bmatrix} \dfrac{\partial p_{k,X}}{\partial p_{k,n}} & \dfrac{\partial p_{k,X}}{\partial p_{k,m}} \\ \dfrac{\partial p_{k,Y}}{\partial p_{k,n}} & \dfrac{\partial p_{k,Y}}{\partial p_{k,m}} \\ \dfrac{\partial p_{k,Z}}{\partial p_{k,n}} & \dfrac{\partial p_{k,Z}}{\partial p_{k,m}} \end{bmatrix} \tag{B-7}$$

where $p_{k,X}$, $p_{k,Y}$, $p_{k,Z}$ are three components of the shell director $\mathbf{p}_i$ along the directions of

global coordinate axes; $p_{k,n}, p_{k,m}$ are two vectorial rotational variables of Node i, which are

the two smallest components among $p_{k,X}$, $p_{k,Y}$, $p_{k,Z}$; $\dfrac{\partial p_{k,n}}{\partial p_{k,n}} = \dfrac{\partial p_{k,m}}{\partial p_{k,m}} = 1$;

$\dfrac{\partial p_{k,n}}{\partial p_{k,m}} = \dfrac{\partial p_{k,m}}{\partial p_{k,n}} = 0$; $\dfrac{\partial p_{k,l}}{\partial p_{k,n}} = -\dfrac{p_{k,n}}{p_{k,l}}$ and $\dfrac{\partial p_{k,l}}{\partial p_{k,m}} = -\dfrac{p_{k,m}}{p_{k,l}}$, $l \neq n \neq m\; l,n,m \in \{X,Y,Z\}$.

If Node k is located at an intersection of non-smooth shells, three vectorial rotational
variables are employed in the global coordinate system, which are the two smallest components of
one vector and the smallest or second smallest component of another vector of an orthogonal triad
oriented initially to three axes of the global coordinate system, and thus

$$\frac{\partial \boldsymbol{\theta}_i}{\partial \mathbf{d}_j^{\mathrm{T}}} = \frac{\partial \mathbf{R}_h}{\partial \mathbf{d}_j^{\mathrm{T}}} \mathbf{R}_i^{\mathrm{T}} \mathbf{R}_{i0} \mathbf{p}_{i0} = \frac{\partial}{\partial \mathbf{d}_j^{\mathrm{T}}} \begin{bmatrix} \mathbf{e}_x^{\mathrm{T}} \\ \mathbf{e}_y^{\mathrm{T}} \end{bmatrix} \mathbf{R}_i^{\mathrm{T}} \mathbf{R}_{i0} \mathbf{p}_{i0} \tag{B-8}$$

$$\frac{\partial \boldsymbol{\theta}_i}{\partial \mathbf{n}_{gj}^{\mathrm{T}}} = \delta_{ij} \mathbf{R}_h \frac{\partial \mathbf{R}_i^{\mathrm{T}}}{\partial \mathbf{n}_{gj}^{\mathrm{T}}} \mathbf{R}_{i0} \mathbf{p}_{i0} = \delta_{ij} \mathbf{R}_h \frac{\partial}{\partial \mathbf{n}_{gj}^{\mathrm{T}}} \begin{bmatrix} \mathbf{e}_{ix} & \mathbf{e}_{iy} & \mathbf{e}_{iz} \end{bmatrix} \mathbf{R}_{i0} \mathbf{p}_{i0} \tag{B-9}$$

The first-order derivative on the right side of Equation (B-8) is the same as Equations (B-4)-(B-6),
and the first-order derivatives on the right side of Equation (B-9) are evaluated as follows

$$\frac{\partial \mathbf{e}_{ix}}{\partial \mathbf{n}_{gi}^{\mathrm{T}}} = \frac{\partial \mathbf{e}_{iy}}{\partial \mathbf{n}_{gi}^{\mathrm{T}}} \times \mathbf{e}_{iz} + \mathbf{e}_{iy} \times \frac{\partial \mathbf{e}_{iz}}{\partial \mathbf{n}_{gj}^{\mathrm{T}}} \tag{B-10}$$

$$\frac{\partial \mathbf{e}_{iy}}{\partial \mathbf{n}_{gi}^{\mathrm{T}}} = \begin{bmatrix} \dfrac{\partial \mathbf{e}_{iy}}{\partial e_{iy,n}} & \dfrac{\partial \mathbf{e}_{iy}}{\partial e_{iy,m}} & \mathbf{0} \end{bmatrix} \tag{B-11}$$

$$\frac{\partial \mathbf{e}_{iz}}{\partial \mathbf{n}_{gi}^{\mathrm{T}}} = \begin{bmatrix} \dfrac{\partial \mathbf{e}_{iz}}{\partial e_{iy,n}} & \dfrac{\partial \mathbf{e}_{iz}}{\partial e_{iy,m}} & \dfrac{\partial \mathbf{e}_{iz}}{\partial e_{iz,n}} \end{bmatrix} \tag{B-12}$$

The components in Equations (B-10)- (B-12) are calculated as follows

$$\frac{\partial e_{iy,n}}{\partial e_{iy,n}} = 1; \qquad \frac{\partial e_{iy,m}}{\partial e_{iy,m}} = 1; \qquad \frac{\partial e_{iy,l}}{\partial e_{iy,n}} = -\frac{e_{iy,n}}{e_{iy,l}} \tag{B-13a,b,c}$$

$$\frac{\partial e_{iy,l}}{\partial e_{iy,m}} = -\frac{e_{iy,m}}{e_{iy,l}} ; \qquad \frac{\partial e_{iz,n}}{\partial e_{iz,n}} = 1 \tag{B-13d,e}$$

$$\frac{\partial e_{iz,l}}{\partial e_{iy,n}} = \frac{1}{1 - e_{iy,n}^2} \left(-\frac{\partial e_{iy,l}}{\partial e_{iy,n}} e_{iy,n} e_{iz,n} - e_{iy,l} e_{iz,n} - s_1 s_3 e_{iy,m} \frac{\partial c_0}{\partial e_{iy,n}} + 2 e_{iz,l} e_{iy,n} \right) \tag{B-13f}$$

$$\frac{\partial e_{iz,l}}{\partial e_{iy,m}} = \frac{1}{1 - e_{iy,n}^2} \left(-\frac{\partial e_{iy,l}}{\partial e_{iy,m}} e_{iy,n} e_{iz,n} - s_1 s_3 c_0 \right) \tag{B-13g}$$

$$\frac{\partial e_{iz,l}}{\partial e_{iz,n}} = \frac{1}{1 - e_{iy,n}^2} \left(-e_{iy,l} e_{iy,n} - s_1 s_3 e_{iy,m} \frac{\partial c_0}{\partial e_{iz,n}} \right) \tag{B-13h}$$

$$\frac{\partial e_{iz,m}}{\partial e_{iy,n}} = -\frac{e_{iz,l}}{e_{iz,m}} \frac{\partial e_{iz,l}}{\partial e_{iy,n}} ; \qquad \frac{\partial e_{iz,m}}{\partial e_{iy,m}} = -\frac{e_{iz,l}}{e_{iz,m}} \frac{\partial e_{iz,l}}{\partial e_{iy,m}} \tag{B-13i,j}$$

$$\frac{\partial e_{iz,m}}{\partial e_{iz,n}} = \frac{-e_{iz,n}}{e_{iz,m}} - \frac{e_{iz,l}}{e_{iz,m}} \frac{\partial e_{iz,l}}{\partial e_{iz,n}} \tag{B-13k}$$

In Equations(B-13f)~(B-13h),

$$c_0 = \sqrt{1 - e_{iy,n}^2 - e_{iz,n}^2} \tag{B-14a}$$

$$\frac{\partial c_0}{\partial e_{iy,n}} = \frac{-e_{iy,n}}{c_0} ; \qquad \frac{\partial c_0}{\partial e_{iz,n}} = \frac{-e_{iz,n}}{c_0} \tag{B-14b,c}$$

The first-order derivatives of the transformation matrix $\mathbf{T}$ with respect to global nodal variables lead to the following sub-matrices:

$$\frac{\partial^2 \mathbf{t}_i}{\partial \mathbf{d}_j^{\mathrm{T}} \partial \mathbf{u}_g^{\mathrm{T}}} = \left[\begin{array}{ccccc} \dfrac{\partial^2 \mathbf{t}_i}{\partial \mathbf{d}_j^{\mathrm{T}} \partial \mathbf{d}_1^{\mathrm{T}}} & 0 & \cdots & \dfrac{\partial^2 \mathbf{t}_i}{\partial \mathbf{d}_j^{\mathrm{T}} \partial \mathbf{d}_6^{\mathrm{T}}} & 0 \end{array} \right] \tag{B-15}$$

$$\frac{\partial^2 \boldsymbol{\theta}_i}{\partial \mathbf{d}_j^{\mathrm{T}} \partial \mathbf{u}_g^{\mathrm{T}}} = \left[\begin{array}{ccccc} \dfrac{\partial^2 \boldsymbol{\theta}_i}{\partial \mathbf{d}_j^{\mathrm{T}} \partial \mathbf{d}_1^{\mathrm{T}}} & \dfrac{\partial^2 \boldsymbol{\theta}_i}{\partial \mathbf{d}_j^{\mathrm{T}} \partial \mathbf{n}_{g1}^{\mathrm{T}}} & \cdots & \dfrac{\partial^2 \boldsymbol{\theta}_i}{\partial \mathbf{d}_j^{\mathrm{T}} \partial \mathbf{d}_6^{\mathrm{T}}} & \dfrac{\partial^2 \boldsymbol{\theta}_i}{\partial \mathbf{d}_j^{\mathrm{T}} \partial \mathbf{n}_{g6}^{\mathrm{T}}} \end{array} \right] \tag{B-16}$$

$$\frac{\partial^2 \boldsymbol{\theta}_i}{\partial \mathbf{n}_{gj}^{\mathrm{T}} \partial \mathbf{u}_g^{\mathrm{T}}} = \left[\begin{array}{ccccc} \dfrac{\partial^2 \boldsymbol{\theta}_i}{\partial \mathbf{n}_{gj}^{\mathrm{T}} \partial \mathbf{d}_1^{\mathrm{T}}} & \dfrac{\partial^2 \boldsymbol{\theta}_i}{\partial \mathbf{n}_{gj}^{\mathrm{T}} \partial \mathbf{n}_{gk}^{\mathrm{T}}} & \cdots & \dfrac{\partial^2 \boldsymbol{\theta}_i}{\partial \mathbf{n}_{gj}^{\mathrm{T}} \partial \mathbf{d}_6^{\mathrm{T}}} & \dfrac{\partial^2 \boldsymbol{\theta}_i}{\partial \mathbf{n}_{gj}^{\mathrm{T}} \partial \mathbf{n}_{g6}^{\mathrm{T}}} \end{array} \right] \tag{B-17}$$

$$\frac{\partial^2 \mathbf{t}_i}{\partial \mathbf{d}_j^{\mathrm{T}} \partial \mathbf{d}_k^{\mathrm{T}}} = \frac{\partial^2 \mathbf{R}}{\partial \mathbf{d}_j^{\mathrm{T}} \partial \mathbf{d}_k^{\mathrm{T}}} \left(\mathbf{d}_i + \mathbf{v}_{i0} \right) + \frac{\partial \mathbf{R}}{\partial \mathbf{d}_j^{\mathrm{T}}} \delta_{ik} \mathbf{I} + \frac{\partial \mathbf{R}}{\partial \mathbf{d}_k^{\mathrm{T}}} \delta_{ij} \mathbf{I}$$

$$= \left[\begin{array}{c} \dfrac{\partial^2 \mathbf{e}_x^{\mathrm{T}}}{\partial \mathbf{d}_j^{\mathrm{T}} \partial \mathbf{d}_k^{\mathrm{T}}} \\[2mm] \dfrac{\partial^2 \mathbf{e}_y^{\mathrm{T}}}{\partial \mathbf{d}_j^{\mathrm{T}} \partial \mathbf{d}_k^{\mathrm{T}}} \\[2mm] \dfrac{\partial^2 \mathbf{e}_z^{\mathrm{T}}}{\partial \mathbf{d}_j^{\mathrm{T}} \partial \mathbf{d}_k^{\mathrm{T}}} \end{array} \right] \left(\mathbf{d}_i + \mathbf{v}_{i0} \right) + \left[\begin{array}{c} \dfrac{\partial \mathbf{e}_x^{\mathrm{T}}}{\partial \mathbf{d}_j^{\mathrm{T}}} \\[2mm] \dfrac{\partial \mathbf{e}_y^{\mathrm{T}}}{\partial \mathbf{d}_j^{\mathrm{T}}} \\[2mm] \dfrac{\partial \mathbf{e}_z^{T}}{\partial \mathbf{d}_j^{\mathrm{T}}} \end{array} \right] \delta_{ik} \mathbf{I} + \left[\begin{array}{c} \dfrac{\partial \mathbf{e}_x^{\mathrm{T}}}{\partial \mathbf{d}_k^{\mathrm{T}}} \\[2mm] \dfrac{\partial \mathbf{e}_y^{\mathrm{T}}}{\partial \mathbf{d}_k^{\mathrm{T}}} \\[2mm] \dfrac{\partial \mathbf{e}_z^{\mathrm{T}}}{\partial \mathbf{d}_k^{\mathrm{T}}} \end{array} \right] \delta_{ij} \mathbf{I} \tag{B-18}$$

If Node k is away from intersections of non-smooth shells, or if it is on a smooth shell mid-surface,

$$\frac{\partial^2 \boldsymbol{\theta}_i}{\partial \mathbf{d}_j^{\mathrm{T}} \partial \mathbf{d}_k^{\mathrm{T}}} = \frac{\partial^2 \mathbf{R}_h}{\partial \mathbf{d}_j^{\mathrm{T}} \partial \mathbf{d}_k^{\mathrm{T}}} \mathbf{p}_i = \left[\begin{array}{c} \dfrac{\partial^2 \mathbf{e}_x^{\mathrm{T}}}{\partial \mathbf{d}_j^{\mathrm{T}} \partial \mathbf{d}_k^{\mathrm{T}}} \\[2mm] \dfrac{\partial^2 \mathbf{e}_y^{\mathrm{T}}}{\partial \mathbf{d}_j^{\mathrm{T}} \partial \mathbf{d}_k^{\mathrm{T}}} \end{array} \right] \mathbf{p}_i \tag{B-19}$$

$$\frac{\partial^2 \boldsymbol{\theta}_i}{\partial \mathbf{d}_j^{\mathrm{T}} \partial \mathbf{n}_{gk}^{\mathrm{T}}} = \frac{\partial \mathbf{R}_h}{\partial \mathbf{d}_j^{\mathrm{T}}} \delta_{ik} \frac{\partial \mathbf{p}_i}{\partial \mathbf{n}_{gk}^{\mathrm{T}}} = \left[\begin{array}{c} \dfrac{\partial \mathbf{e}_x^{\mathrm{T}}}{\partial \mathbf{d}_j^{\mathrm{T}}} \\[2mm] \dfrac{\partial \mathbf{e}_y^{\mathrm{T}}}{\partial \mathbf{d}_j^{\mathrm{T}}} \end{array} \right] \delta_{ik} \frac{\partial \mathbf{p}_i}{\partial \mathbf{n}_{gk}^{\mathrm{T}}} \tag{B-20}$$

$$\frac{\partial^2 \boldsymbol{\theta}_i}{\partial \mathbf{n}_{gj}^{\mathrm{T}} \partial \mathbf{n}_{gk}^{\mathrm{T}}} = \mathbf{R}_h \delta_{ij} \delta_{ik} \frac{\partial^2 \mathbf{p}_i}{\partial \mathbf{n}_{gj}^{\mathrm{T}} \partial \mathbf{n}_{gk}^{\mathrm{T}}} \tag{B-21}$$

$$\frac{\partial^2 \mathbf{e}_x}{\partial \mathbf{d}_j^{\mathrm{T}} \partial \mathbf{d}_k^{\mathrm{T}}} = -\frac{1}{\left|\mathbf{v}_{12}\right|^3}\left[\frac{\partial \mathbf{v}_{12}}{\partial \mathbf{d}_j^{\mathrm{T}}} \otimes \mathbf{v}_{12} \frac{\partial \mathbf{v}_{12}}{\partial \mathbf{d}_k^{\mathrm{T}}} + \frac{\partial \mathbf{v}_{12}}{\partial \mathbf{d}_k^{\mathrm{T}}} \otimes \mathbf{v}_{12} \frac{\partial \mathbf{v}_{12}}{\partial \mathbf{d}_j^{\mathrm{T}}} + \mathbf{v}_{12} \otimes \left(\frac{\partial \mathbf{v}_{12}}{\partial \mathbf{d}_j^{\mathrm{T}}}\right)^{\mathrm{T}} \frac{\partial \mathbf{v}_{12}}{\partial \mathbf{d}_k^{\mathrm{T}}}\right]$$

$$+ \frac{3\mathbf{v}_{12}}{\left|\mathbf{v}_{12}\right|^5} \otimes \mathbf{v}_{12} \frac{\partial \mathbf{v}_{12}}{\partial \mathbf{d}_j^{\mathrm{T}}} \otimes \mathbf{v}_{12} \frac{\partial \mathbf{v}_{12}}{\partial \mathbf{d}_k^{\mathrm{T}}} \tag{B-22}$$

$$\frac{\partial^2 \mathbf{e}_z}{\partial \mathbf{d}_j^{\mathrm{T}} \partial \mathbf{d}_k^{\mathrm{T}}} = \left[\frac{\mathbf{I}}{\left|\mathbf{v}_{12} \times \mathbf{v}_{13}\right|} - \frac{\left(\mathbf{v}_{12} \times \mathbf{v}_{13}\right) \otimes \left(\mathbf{v}_{12} \times \mathbf{v}_{13}\right)}{\left|\mathbf{v}_{12} \times \mathbf{v}_{13}\right|^3}\right]\left(\frac{\partial \mathbf{v}_{12}}{\partial \mathbf{d}_j^{\mathrm{T}}} \times \frac{\partial \mathbf{v}_{13}}{\partial \mathbf{d}_k^{\mathrm{T}}} + \frac{\partial \mathbf{v}_{12}}{\partial \mathbf{d}_k^{\mathrm{T}}} \times \frac{\partial \mathbf{v}_{13}}{\partial \mathbf{d}_j^{\mathrm{T}}}\right)$$

$$- \left(\frac{\partial \mathbf{v}_{12}}{\partial \mathbf{d}_j^{\mathrm{T}}} \times \mathbf{v}_{13} + \mathbf{v}_{12} \times \frac{\partial \mathbf{v}_{13}}{\partial \mathbf{d}_j^{\mathrm{T}}}\right) \otimes \frac{\left(\mathbf{v}_{12} \times \mathbf{v}_{13}\right)}{\left|\mathbf{v}_{12} \times \mathbf{v}_{13}\right|^3}\left(\frac{\partial \mathbf{v}_{12}}{\partial \mathbf{d}_k^{\mathrm{T}}} \times \mathbf{v}_{13} + \mathbf{v}_{12} \times \frac{\partial \mathbf{v}_{13}}{\partial \mathbf{d}_k^{\mathrm{T}}}\right)$$

$$- \frac{\left(\mathbf{v}_{12} \times \mathbf{v}_{13}\right)}{\left|\mathbf{v}_{12} \times \mathbf{v}_{13}\right|^3} \otimes \left(\frac{\partial \mathbf{v}_{12}}{\partial \mathbf{d}_j^{\mathrm{T}}} \times \mathbf{v}_{13} + \mathbf{v}_{12} \times \frac{\partial \mathbf{v}_{13}}{\partial \mathbf{d}_j^{\mathrm{T}}}\right)^{\mathrm{T}}\left(\frac{\partial \mathbf{v}_{12}}{\partial \mathbf{d}_k^{\mathrm{T}}} \times \mathbf{v}_{13} + \mathbf{v}_{12} \times \frac{\partial \mathbf{v}_{13}}{\partial \mathbf{d}_k^{\mathrm{T}}}\right)$$

$$- \left(\frac{\partial \mathbf{v}_{12}}{\partial \mathbf{d}_k^{\mathrm{T}}} \times \mathbf{v}_{13} + \mathbf{v}_{12} \times \frac{\partial \mathbf{v}_{13}}{\partial \mathbf{d}_k^{\mathrm{T}}}\right) \otimes \frac{\left(\mathbf{v}_{12} \times \mathbf{v}_{13}\right)}{\left|\mathbf{v}_{12} \times \mathbf{v}_{13}\right|^3}\left(\frac{\partial \mathbf{v}_{12}}{\partial \mathbf{d}_j^{\mathrm{T}}} \times \mathbf{v}_{13} + \mathbf{v}_{12} \times \frac{\partial \mathbf{v}_{13}}{\partial \mathbf{d}_j^{\mathrm{T}}}\right)$$

$$+ \frac{3\left(\mathbf{v}_{12} \times \mathbf{v}_{13}\right) \otimes \left(\mathbf{v}_{12} \times \mathbf{v}_{13}\right)}{\left|\mathbf{v}_{12} \times \mathbf{v}_{13}\right|^5}\left(\frac{\partial \mathbf{v}_{12}}{\partial \mathbf{d}_j} \times \mathbf{v}_{13} + \mathbf{v}_{12} \times \frac{\partial \mathbf{v}_{13}}{\partial \mathbf{d}_j}\right) \otimes \left(\mathbf{v}_{12} \times \mathbf{v}_{13}\right)\left(\frac{\partial \mathbf{v}_{12}}{\partial \mathbf{d}_k} \times \mathbf{v}_{13} + \mathbf{v}_{12} \times \frac{\partial \mathbf{v}_{13}}{\partial \mathbf{d}_k}\right)$$

$$\tag{B-23}$$

$$\frac{\partial^2 \mathbf{e}_y}{\partial \mathbf{d}_j^{\mathrm{T}} \partial \mathbf{d}_k^{\mathrm{T}}} = \frac{\partial^2 \mathbf{e}_z}{\partial \mathbf{d}_j^{\mathrm{T}} \partial \mathbf{d}_k^{\mathrm{T}}} \times \mathbf{e}_x + \mathbf{e}_z \times \frac{\partial^2 \mathbf{e}_x}{\partial \mathbf{d}_j^{\mathrm{T}} \partial \mathbf{d}_k^{\mathrm{T}}} + \frac{\partial \mathbf{e}_z}{\partial \mathbf{d}_j^{\mathrm{T}}} \times \frac{\partial \mathbf{e}_x}{\partial \mathbf{d}_k^{\mathrm{T}}} + \frac{\partial \mathbf{e}_z}{\partial \mathbf{d}_k^{\mathrm{T}}} \times \frac{\partial \mathbf{e}_x}{\partial \mathbf{d}_j^{\mathrm{T}}} \tag{B-24}$$

$$\frac{\partial^2 \mathbf{p}_i}{\partial \mathbf{n}_{gi}^{\mathrm{T}\,2}} = \begin{bmatrix} \dfrac{\partial^2 \mathbf{p}_i}{\partial p_{i,n_i}^2} & \dfrac{\partial^2 \mathbf{p}_i}{\partial p_{i,n_i} \partial p_{i,m_i}} \\ \dfrac{\partial^2 \mathbf{p}_i}{\partial p_{i,m_i} \partial p_{i,n_i}} & \dfrac{\partial^2 \mathbf{p}_i}{\partial p_{i,m_i}^2} \end{bmatrix} \tag{B-25}$$

$$\frac{\partial^2 \mathbf{p}_i}{\partial p_{i,n_i}^2} = \begin{Bmatrix} \dfrac{\partial^2 p_{i,X}}{\partial p_{i,n_i}^2} \\ \dfrac{\partial^2 p_{i,Y}}{\partial p_{i,n_i}^2} \\ \dfrac{\partial^2 p_{i,Z}}{\partial p_{i,n_i}^2} \end{Bmatrix}, \quad \frac{\partial^2 \mathbf{p}_i}{\partial p_{i,m_i}^2} = \begin{Bmatrix} \dfrac{\partial^2 p_{i,X}}{\partial p_{i,m_i}^2} \\ \dfrac{\partial^2 p_{i,Y}}{\partial p_{i,m_i}^2} \\ \dfrac{\partial^2 p_{i,Z}}{\partial p_{i,m_i}^2} \end{Bmatrix}, \quad \frac{\partial^2 \mathbf{p}_i}{\partial p_{i,n_i} \partial p_{i,m_i}} = \begin{Bmatrix} \dfrac{\partial^2 p_{i,X}}{\partial p_{i,n_i} \partial p_{i,m_i}} \\ \dfrac{\partial^2 p_{i,Y}}{\partial p_{i,n_i} \partial p_{i,m_i}} \\ \dfrac{\partial^2 p_{i,Z}}{\partial p_{i,n_i} \partial p_{i,m_i}} \end{Bmatrix} \tag{B-26a,b,c}$$

$$\frac{\partial^2 p_{i,l_i}}{\partial p_{i,n_i}^2} = -\frac{1}{p_{i,l_i}} - \frac{p_{i,n_i}^2}{p_{i,l_i}^3}, \frac{\partial^2 p_{i,l_i}}{\partial p_{i,m_i}^2} = -\frac{1}{p_{i,l_i}} - \frac{p_{i,m_i}^2}{p_{i,l_i}^3}, \frac{\partial^2 p_{i,l_i}}{\partial p_{i,n_i} \partial p_{i,m_i}} = -\frac{p_{i,n_i} p_{i,m_i}}{p_{i,l_i}^3} \quad \text{(B-27a,b,c)}$$

where second-order derivatives of the other two components with respect to the vectorial rotational variables are equal to zero.

If Node k is located at an intersection of non-smooth shells,

$$\frac{\partial^2 \boldsymbol{\theta}_i}{\partial \mathbf{d}_j^T \partial \mathbf{d}_k^T} = \frac{\partial^2 \mathbf{R}_h}{\partial \mathbf{d}_j^T \partial \mathbf{d}_k^T} \mathbf{R}_i^T \mathbf{R}_{i0} \mathbf{p}_{i0} = \begin{bmatrix} \dfrac{\partial^2 \mathbf{e}_x^T}{\partial \mathbf{d}_j^T \partial \mathbf{d}_k^T} \\ \dfrac{\partial^2 \mathbf{e}_y^T}{\partial \mathbf{d}_j^T \partial \mathbf{d}_k^T} \end{bmatrix} \mathbf{R}_i^T \mathbf{R}_{i0} \mathbf{p}_{i0} \quad \text{(B-28)}$$

The second-order derivatives on the right hand side of Equation (B-28) are the same as Equations (B22)-(B24).

$$\frac{\partial^2 \boldsymbol{\theta}_i}{\partial \mathbf{d}_j^T \partial \mathbf{n}_{gk}^T} = \frac{\partial \mathbf{R}_h}{\partial \mathbf{d}_j^T} \delta_{ik} \frac{\partial \mathbf{R}_i^T}{\partial \mathbf{n}_{gk}^T} \mathbf{R}_{i0} \mathbf{p}_{i0} = \begin{bmatrix} \dfrac{\partial \mathbf{e}_x^T}{\partial \mathbf{d}_j^T} \\ \dfrac{\partial \mathbf{e}_y^T}{\partial \mathbf{d}_j^T} \end{bmatrix} \delta_{ik} \begin{bmatrix} \dfrac{\partial \mathbf{e}_{ix}}{\partial \mathbf{n}_{gk}^T} & \dfrac{\partial \mathbf{e}_{iy}}{\partial \mathbf{n}_{gk}^T} & \dfrac{\partial \mathbf{e}_{iz}}{\partial \mathbf{n}_{gk}^T} \end{bmatrix} \mathbf{R}_{i0} \mathbf{p}_{i0} \quad \text{(B-29)}$$

$$\frac{\partial^2 \boldsymbol{\theta}_i}{\partial \mathbf{n}_{gj}^T \partial \mathbf{n}_{gk}^T} = \mathbf{R}_h \delta_{ij} \delta_{ik} \frac{\partial^2 \mathbf{R}_i^T}{\partial \mathbf{n}_{gj}^T \partial \mathbf{n}_{gk}^T} \mathbf{R}_{i0} \mathbf{p}_{i0}$$

$$= \mathbf{R}_h \delta_{ij} \delta_{ik} \begin{bmatrix} \dfrac{\partial^2 \mathbf{e}_{ix}}{\partial \mathbf{n}_{gj}^T \partial \mathbf{n}_{gk}^T} & \dfrac{\partial^2 \mathbf{e}_{iy}}{\partial \mathbf{n}_{gj}^T \partial \mathbf{n}_{gk}^T} & \dfrac{\partial^2 \mathbf{e}_{iz}}{\partial \mathbf{n}_{gj}^T \partial \mathbf{n}_{gk}^T} \end{bmatrix} \mathbf{R}_{i0} \mathbf{p}_{i0} \quad \text{(B-30)}$$

$$\frac{\partial^2 \mathbf{e}_{ix}}{\partial \mathbf{n}_{gj}^T \partial \mathbf{n}_{gk}^T} = \frac{\partial^2 \mathbf{e}_{iy}}{\partial \mathbf{n}_{gj}^T \partial \mathbf{n}_{gk}^T} \times \mathbf{e}_{iz} + \mathbf{e}_{iy} \times \frac{\partial^2 \mathbf{e}_{iz}}{\partial \mathbf{n}_{gj}^T \partial \mathbf{n}_{gk}^T} + \frac{\partial \mathbf{e}_{iy}}{\partial \mathbf{n}_{gj}^T} \times \frac{\partial \mathbf{e}_{iz}}{\partial \mathbf{n}_{gk}^T} + \frac{\partial \mathbf{e}_{iy}}{\partial \mathbf{n}_{gk}^T} \times \frac{\partial \mathbf{e}_{iz}}{\partial \mathbf{n}_{gi}^T} \quad \text{(B-31)}$$

The first-order derivatives in Equations (B-29) and (B-31) are calculated as Equations (B-4)-(B-6), and Equations (B-10)-(B-14). The second-order derivatives in Equations (B-30) and (B-31) are calculated as follows

$$\frac{\partial^2 e_{iy,l}}{\partial^2 e_{iy,n}} = -\frac{e_{iy,n}^2}{e_{iy,l}^3} - \frac{1}{e_{iy,l}}; \quad \frac{\partial^2 e_{iy,l}}{\partial e_{iy,n} \partial e_{iy,m}} = -\frac{e_{iy,n} e_{iy,m}}{e_{iy,l}^3}; \quad \frac{\partial^2 e_{iy,l}}{\partial^2 e_{iy,m}} = -\frac{e_{iy,m}^2}{e_{iy,l}^3} - \frac{1}{e_{iy,l}} \quad \text{(B-32a,b,c)}$$

$$\frac{\partial^2 c_0}{\partial^2 e_{iy,n}} = -\frac{e_{iy,n}^2}{c_0^3} - \frac{1}{c_0}; \quad \frac{\partial^2 c_0}{\partial e_{iy,n} \partial e_{iz,n}} = -\frac{e_{iy,n} e_{iz,n}}{c_0^3}; \quad \frac{\partial^2 c_0}{\partial^2 e_{iz,n}} = -\frac{e_{iz,n}^2}{c_0^3} - \frac{1}{c_0} \quad \text{(B-32d,e,f)}$$

$$\frac{\partial^2 e_{iz,l}}{\partial e_{iy,n}^2} = \frac{1}{1-e_{iy,n}^2}\left\{ -\left[\frac{\partial^2 e_{iy,l}}{\partial e_{iy,n}^2} e_{iy,n} + 2\frac{\partial e_{iy,l}}{\partial e_{iy,n}}\right]e_{iz,n} - s_1 s_3 e_{iy,m} \frac{\partial^2 c_0}{\partial e_{iy,n}^2} + 2e_{iy,n}\frac{\partial e_{iz,l}}{\partial e_{iy,n}} + 2e_{iz,l}\right\}$$

$$+ \frac{2e_{iy,n}}{1-e_{iy,n}^2}\frac{\partial e_{iz,l}}{\partial e_{iy,n}} \quad \text{(B-32g)}$$

$$\frac{\partial^2 e_{iz,l}}{\partial e_{iy,n} \partial e_{iy,m}} = \frac{-1}{1-e_{iy,n}^2}\left[\left(\frac{\partial^2 e_{iy,l}}{\partial e_{iy,n} \partial e_{iy,m}} e_{iy,n} + \frac{\partial e_{iy,l}}{\partial e_{iy,m}}\right)e_{iz,n} + s_1 s_3 \frac{\partial c_0}{\partial e_{iy,n}} - 2e_{iy,n}\frac{\partial e_{iz,l}}{\partial e_{iy,m}}\right] \text{(B-32h)}$$

$$\frac{\partial^2 e_{iz,l}}{\partial e_{iy,n} \partial e_{iz,n}} = \frac{-1}{1-e_{iy,n}^2}\left(e_{iy,n}\frac{\partial e_{iy,l}}{\partial e_{iy,n}} + e_{iy,l} + s_1 s_3 e_{iy,m}\frac{\partial^2 c_0}{\partial e_{iy,n} \partial e_{iz,n}} + 2e_{iy,n}\frac{\partial e_{iz,l}}{\partial e_{iz,n}}\right) \text{(B-32i)}$$

$$\frac{\partial^2 e_{iz,l}}{\partial e_{iy,m}^2} = -\frac{e_{iy,n} e_{iz,n}}{1-e_{iy,n}^2}\frac{\partial^2 e_{iy,l}}{\partial e_{iy,m}^2} \quad \text{(B-32j)}$$

$$\frac{\partial^2 e_{iz,l}}{\partial e_{iy,m} \partial e_{iz,n}} = \frac{1}{1-e_{iy,n}^2}\left(-\frac{\partial e_{iy,l}}{\partial e_{iy,m}} e_{iy,n} - s_1 s_3 \frac{\partial c_0}{\partial e_{iz,n}}\right) \quad \text{(B-32k)}$$

$$\frac{\partial^2 e_{iz,l}}{\partial e_{iz,n}^2} = \frac{-s_1 s_3 e_{iy,m}}{1-e_{iy,n}^2}\frac{\partial^2 c_0}{\partial e_{iz,n}^2} \quad \text{(B-32l)}$$

$$\frac{\partial^2 e_{iz,m}}{\partial e_{iy,n}^2} = -\left[\frac{1}{e_{iz,m}}\left(\frac{\partial e_{iz,l}}{\partial e_{iy,n}}\right)^2 + \frac{e_{iz,l}}{e_{iz,m}}\frac{\partial^2 e_{iz,l}}{\partial e_{iy,n}^2}\right] - \frac{1}{e_{iz,m}}\left(\frac{\partial e_{iz,m}}{\partial e_{iy,n}}\right)^2 \quad \text{(B-32m)}$$

$$\frac{\partial^2 e_{iz,m}}{\partial e_{iy,n} \partial e_{iy,m}} = -\frac{1}{e_{iz,m}}\frac{\partial e_{iz,l}}{\partial e_{iy,n}}\frac{\partial e_{iz,l}}{\partial e_{iy,m}} - \frac{e_{iz,l}}{e_{iz,m}}\frac{\partial^2 e_{iz,l}}{\partial e_{iy,n} \partial e_{iy,m}} - \frac{1}{e_{iz,m}}\frac{\partial e_{iz,m}}{\partial e_{iy,n}}\frac{\partial e_{iz,m}}{\partial e_{iy,m}} \quad \text{(B-32n)}$$

$$\frac{\partial^2 e_{iz,m}}{\partial e_{iy,n} \partial e_{iz,n}} = -\frac{1}{e_{iz,m}}\frac{\partial e_{iz,l}}{\partial e_{iy,n}}\frac{\partial e_{iz,l}}{\partial e_{iz,n}} - \frac{e_{iz,l}}{e_{iz,m}}\frac{\partial^2 e_{iz,l}}{\partial e_{iy,n} \partial e_{iz,n}} - \frac{1}{e_{iz,m}}\frac{\partial e_{iz,m}}{\partial e_{iy,n}}\frac{\partial e_{iz,m}}{\partial e_{iz,n}} \quad \text{(B-32o)}$$

$$\frac{\partial^2 e_{iz,m}}{\partial e_{iy,m}^2} = -\frac{1}{e_{iz,m}}\left(\frac{\partial e_{iz,l}}{\partial e_{iy,m}}\right)^2 - \frac{e_{iz,l}}{e_{iz,m}}\frac{\partial^2 e_{iz,l}}{\partial e_{iy,m}^2} - \frac{1}{e_{iz,m}}\left(\frac{\partial e_{iz,m}}{\partial e_{iy,m}}\right)^2 \quad \text{(B-32p)}$$

$$\frac{\partial^2 e_{iz,m}}{\partial e_{iy,m} \partial e_{iz,n}} = -\frac{1}{e_{iz,m}} \frac{\partial e_{iz,l}}{\partial e_{iy,m}} \frac{\partial e_{iz,l}}{\partial e_{iz,n}} - \frac{e_{iz,l}}{e_{iz,m}} \frac{\partial^2 e_{iz,l}}{\partial e_{iy,m} \partial e_{iz,n}} - \frac{1}{e_{iz,m}} \frac{\partial e_{iz,m}}{\partial e_{iy,m}} \frac{\partial e_{iz,m}}{\partial e_{iz,n}} \quad \text{(B-32q)}$$

$$\frac{\partial^2 e_{iz,m}}{\partial e_{iz,n}^2} = -\frac{1}{e_{iz,m}} - \frac{e_{iz,l}}{e_{iz,m}} \frac{\partial^2 e_{iz,l}}{\partial e_{iz,n}^2} - \frac{1}{e_{iz,m}} \left(\frac{\partial e_{iz,l}}{\partial e_{iz,n}} \right)^2 - \frac{1}{e_{iz,m}} \left(\frac{\partial e_{iz,m}}{\partial e_{iz,n}} \right)^2 \quad \text{(B-32r)}$$

Acknowledgements

References

1. Altenbach, H.,Eremeyev, V.: Shell-like Structures: Advanced Theories and Applications. Springer (2017). https://link.springer.com/book/10.1007/978-3-319-42277-0

2. Pietraszkiewicz, W., Witkowski, W.: Shell Structures: Theory and Applications, Volume 4. CRC Press,Balkema(2018).https://doi.org/10.1201/9781315166605

3. Altenbach, H., Chróścielewski, J., Eremeev V., Wiśniewski K.: Recent Developments in the Theory of Shells. Springer(2019).https://doi.org/10.1007/978-3-030-17747-8

4. Pietraszkiewicz, W., Konopinska, V.: Junctions in shell structures: A review. Thin Wall. Struct.**95**, 310-334 (2015). https://doi.org/10.1016/j.tws.2015.07.010

5.Lu, X.Z., Tian, Y., Sun, C.J., Zhang, S. H.: Development and Application of a High-Performance Triangular Shell Element and an Explicit Algorithm in OpenSees for Strongly Nonlinear Analysis. CMES-Comp. Model Eng., **120**(3), 561-582. (2019) https://doi.org/10.32604/cmes.2019.04770

6. Schellenberg, A.H., Huang, Y. L., Mahin, S. A.: Structural Finite Element Software Coupling Using Adapter Elements. CMES-Comp. Model Eng.**120**(3), 719-737 (2019) https://doi.org/10.32604/cmes.2019.04835

7. Argyris, J. H., Balmer, H., Doltsinis, J. S., Dunne, P. C.,Haase,M.,Kleiber, M.,Malejannakis, G. A.,Mlejnek, H. P., Muller, M.,Scharpf, D. W.: Finite-element method - natural approach.Comput. Methods Appl. Mech. Eng.**17-8**(1), 1-106 (1979). https://doi.org/10.1016/0045-7825 (79)90083-5

8. Simo, J. C.: A finite strain beam formulation - the 3-dimensional dynamic problem. Part I. Comput. Methods Appl. Mech. Eng. **49**(1), 55-70 (1985). https://doi.org/10.1016/0045-7825(85)90050-7

9. Ibrahimbegovic, A.: Stress resultant geometrically nonlinear shell theory with drilling rotations .1. A consistent formulation. Comput. Methods Appl. Mech. Eng. **118**(3-4), 265-284 (1994). https://doi.org/10.1016/0045-7825(94)90003-5

10. Ibrahimbegovic, A., Frey, F.: Stress resultant geometrically nonlinear shell theory with drilling rotations .2. Computational aspects. Comput. Methods Appl. Mech. Eng. **118**(3-4), 285-308 (1994). https://doi.org/10.1016/0045-7825(94)90004-3

11. Ibrahimbegovic, A., Frey, F.: Stress resultant geometrically nonlinear shell theory with drilling rotations .3. Linearized kinematics. Int. J. Numer. Methods Eng. **37**(21), 3659-3683 (1994). https://doi.org/10.1002/nme.1620372106

12. Chroscielewski, J., Kreja, I., Sabik, A., Witkowski, W.: Modeling of composite shells in 6-parameter nonlinear theory with drilling degree of freedom. Mech. Adv. Mater. Struct.**18**(6), 403-419 (2011). https://doi.org/10.1080/15376494.2010.524972

13. Chróścielewski, J., Makowski, J., & Stumpf, H.: Genuinely resultant shell finite elements accounting for geometric and material non-linearity. Int. J. Numer. Methods Eng., 35(1), 63-94. (1992). doi:10.1002/nme.1620350105

14. Fox, D. D., Simo, J. C.: A drill rotation formulation for geometrically exact shells. Comput. Methods Appl. Mech. Eng. **98**(3), 329-343 (1992). https://doi.org/10.1016/0045-7825(92)90002-2

15. Witkowski, W.: 4-Node combined shell element with semi-EAS-ANS strain interpolations in 6-parameter shell theories with drilling degrees of freedom. Comput. Mech. **43**(2), 307-319 (2009). https://doi.org/10.1007/s00466-008-0307-x

16. Ibrahimbegovic, A., Wilson, E. L.: A unified formulation for triangular and quadrilateral flat shell finite-elements with 6 nodal degrees of freedom. Commun. Appl. Numer. M.**7**(1), 1-9 (1991). https://doi.org/10.1002/cnm.1630070102

17. Kebari, H., Cassell, A. C.: Non-conforming modes stabilization of a 9-node stress-resultant degenerated shell element with drilling freedom. Comput. Struct. **40**(3), 569-580 (1991). https://doi.org/10.1016/0045-7949(91)90227-D

18. Simo, J. C., Fox, D. D., Rifai, M. S.: On a stress resultant geometrically exact shell-model. 2. The linear-theory - computational aspects. Comput. Methods Appl. Mech. Eng. **73**(1), 53-92 (1989). https://doi.org/10.1016/0045-7825(89)90098-4

19. Dornisch, W., Klinkel, S.: Treatment of Reissner-Mindlin shells with kinks without the need for drilling rotation stabilization in an isogeometric framework. Comput. Methods Appl. Mech. Eng. **276**, 35-66 (2014). https://doi.org/10.1016/j.cma.2014.03.017

20. Vu-Quoc, L., Tan, X. G.: Optimal solid shells for non-linear analyses of multilayer composites. I. Statics. Comput. Methods Appl. Mech. Eng. **192**(9-10), 975-1016 (2003). https://doi.org/10.1016/S0045-7825(02)00435-8

21. Hauptmann, R., Schweizerhof, K.: A systematic development of 'solid-shell' element formulations for linear and non-linear analyses employing only displacement degrees of freedom, Int. J. Numer. Methods Eng. **42**(1) 49-69 (1998). https://doi.org/10.1002/(SICI)1097-0207(19980515)42:1<49::AID-NME349>3.3.CO;2-U

22. Sze, K. Y., Chan, W. K., Pian, T. H. H.: An eight-node hybrid-stress solid-shell element for geometric non-linear analysis of elastic shells. Int. J. Numer. Methods Eng. **55**(7), 853-878

(2002). https://doi.org/10.1002/nme.535

23. Sze, K.Y., Zheng, S. J.: A stabilized hybrid-stress solid element for geometrically nonlinear homogeneous and laminated shell analyses, Comput. Methods Appl. Mech. Eng. **191**(17-18), 1945-1966 (2002). https://doi.org/10.1016/S0045-7825(01)00362-0

24. Sze, K.Y., Yao, L. Q.: A hybrid stress ANS solid-shell element and its generalization for smart structure modelling. Part I - solid-shell element formulation, Int. J. Numer. Methods Eng. **48**(4), 545-564 (2000). https://doi.org/ 10.1002/(SICI)1097-0207(20000610)48:4<545::AID-NME889>3.3.CO;2-Y

25. Li, Z.X., Li, T.Z., Vu-Quoc, L., Izzuddin B.A., Zhuo,X.,Fang, Q.L. A 9-node co-rotational curved quadrilateral shell element for smooth,folded and multi-shell structures. Int. J. Numer. Methods Eng.**116**(8): 570-600(2018). https://doi.org/10.1002/nme.5936

26. Li, Z.X., Xiang, Y., Izzuddin, B.A., Vu-Quoc, L., Zhuo, X., Zhang, C.J.: A 6-node co-rotational triangular elasto-plastic shell element. Comput. Mech.**55**(5): 837-859 (2015).https://doi.org/ 10.1007/s00466-015-1138-1

27. Li ZX, Vu-Quoc L.: An efficient co-rotational formulation for curved triangular shell element. Int. J. Numer. Methods Eng.**72**(9):1029-1062 (2007).https://doi.org/ 10.1002/nme.2064.

28. Koschnick F., Bischoff M.,Camprubi N.,Bletzinger K.U.: The discrete strain gap method and membrane locking. Comput. Methods Appl. Mech. Eng. 194(21-24), 2444-2463. (2005). https://doi: 10.1016/j.cma.2004.07.040

29. Bletzinger K. U., Bischoff M.,RammE.:A unified approach for shear-locking-free triangular and rectangular shell finite elements.Comput. Struct. **75**(3), 321-334 (2000). https://doi.org/10.1016/S0045-7949(99)00140-6

30. Brank B., Peric D., Damjanic F. B.: on implementation of a nonlinear 4 node shell finite-element for thin multilayered elastic shells.Comput. Mech. **16**(5), 341-359 (1995). https://doi.org/ 10.1007/BF00350723

31. Parisch H.: An investigation of a finite rotation 4 node assumed strain shell element. Int. J. Numer. Methods Eng.**31**(1), 127-150 (1991). https://doi.org/ 10.1002/nme.1620310108

32. Sze K. Y., Liu X.H., Lo S. H.: Popular benchmark problems for geometric nonlinear analysis of shells. Finite Elem. Anal. Des. **40**(11), 1551-1569 (2004). https://doi.org/ 10.1016/j.finel.2003.11.001

33. Xiong H., Maldonado E. G., Hamila N., Boisse P.: A prismatic solid-shell finite element based on a DKT approach with efficient calculation of through the thickness deformation. Finite Elem. Anal. Des. **151**, 18-33 (2018). https://doi.org/10.1016/j.finel.2018.08.003

34. ANSYS Academic Research Mechanical, Release 19.3, 2019.

35. Chroscielewski, J., Makowski, J., Stumpf, H.: Finite element analysis of smooth, folded and multi-shell structures.Comput. Methods Appl. Mech. Eng.**141**(1-2), 1-46 (1997). https://doi.org/10.1016/S0045-7825(96)01046-8

36. ANSYS, Inc. Theory Reference Release 18.0. December 2016.

37. Crisfield, M. A.: Nonlinear Finite Element Analysis of Solid and Structures, Vol.1: Essentials.

Wiley, Chichester (1991)

38. Crisfield, M.A.: Nonlinear Finite Element Analysis of Solid and Structures, Vol.2: Advanced topics. Wiley, Chichester (1996)

39. Yang, H. T. Y.,Saigal, S., Masud, A., Kapania, R. K.: Survey of recent shell finite elements. Int. J. Numer. Methods Eng.**47**, 101-127 (2000). https://doi.org/10.1002/(SICI)1097-0207 (20000110/30)47:1/3<101::AID-NME763>3.0.CO;2-C

40. Izzuddin, B. A., Liang, Y.: Bisector and zero-macrospin co-rotational systems for shell elements. Int. J. Numer. Methods Eng. **105**(4), 286-320 (2016). https://doi.org/ 10.1002/nme.4978

41. Tang, Y. Q., Liu, Y. P., & Chan, S. L.: Element-independent pure deformational and co-rotational methods for triangular shell elements in geometrically nonlinear analysis. Int. J. Struct. Stab. Dy., **18**(5). (2018).https://doi.org/10.1142/S0219455418500657.

42. Simo, J. C., Tarnow, N.: A new energy and momentum conserving algorithm for the non-linear dynamics of shells.Int. J. Numer. Methods Eng. **37**(15), 2527-2549 (1994). https://doi.org/10.1002/nme.1620371503

43. Simo, J. C., Rifai, M. S., Fox, D. D.: On a stress resultant geometrically exact shell-model .6. Conserving algorithms for nonlinear dynamics. Int. J. Numer. Methods Eng.**34**(1), 117-164 (1992). https://doi.org/10.1002/nme.1620340108

44. Yang, Y. B., Shieh, M. S.: Solution method for nonlinear problems with multiple critical points. AIAA J. **28**(12), 2110-2116 (1990). https://doi.org/10.2514/3.10529

45. Klinkel, S., Gruttmann, F., Wagner, W.: A mixed shell formulation accounting for thickness strains and finite strain 3D-material models. Int. J. Numer. Methods Eng.**74**(6), 945-970, (2008). https://doi.org/10.1002/nme.2199